KERNFORSCHUNGSZENTRUM

KARLSRUHE

April/Mai 1971

KFK 1443

Institut für Angewandte Kernphysik

Neutron Scattering from ^{15}N
(I). R-matrix and Phase-shift Analysis
(II). Coupled Channel Calculations

S. Cierjacks, G. J. Kirouac, J. Nebe
und
H. Dubenkopf, R. Putzki, B. Zeitnitz, Universität Hamburg
C. B. Dover, Universität und MPI für Kernphysik, Heidelberg

GESELLSCHAFT FÜR KERNFORSCHUNG M. B. H.

KARLSRUHE

2.C

Nuclear Physics **A166** (1971) 443—460; © *North-Holland Publishing Co., Amsterdam*

NEUTRON SCATTERING FROM ^{15}N

(I). *R*-matrix and phase-shift analyses

B. ZEITNITZ, H. DUBENKROPP and R. PUTZKI

II. Institut für Experimentalphysik, Universität Hamburg

G. J. KIROUAC, S. CIERJACKS and J. NEBE

Institut für Angewandte Kernphysik, Kernforschungszentrum Karlsruhe

CARL B. DOVER

Institut für Theoretische Physik der Universität und Max-Planck-Institut für Kernphysik, Heidelberg

Received 23 September 1970

(Revised 17 February 1971)

Abstract: The total neutron cross section of ^{15}N was measured in the neutron energy range between 0.9 and 32 MeV. Between 0.8 and 3.1 MeV angular distribution and polarization measurements were performed. Assignments for levels in ^{16}N up to $E_x = 6.7$ MeV could be determined using *R*-matrix and phase-shift analyses. The positions of the $d_{\frac{3}{2}}$ single-particle resonances were established. Above $E_x = 6.7$ MeV estimates of the angular momenta were obtained from the total cross section by the $2J+1$ rule.

E

NUCLEAR REACTIONS ^{15}N(n), (n, n), $E = 0.9-32$ MeV; measured $\sigma_{nT}(E)$, $\sigma(E)$, $\sigma(E, \theta)$, $P(E, \theta)$. *R*-matrix and phase-shift analyses. ^{16}N deduced resonances, J, π, Γ. Enriched target.

1. Introduction

The n+^{15}N reaction has been the subject of much experimental [1-6]) and theoretical [7-14]) study. However, previous experimental work has been restricted to the energy region below about $E_n = 6$ MeV and gave partially contradictory results with respect to energy and spin assignments of levels in ^{16}N.

From the point of view of the independent-particle shell model, the reaction n+^{15}N is a favourable case for study, since the $\frac{1}{2}^-$ ground state and the low-lying $\frac{3}{2}^-$ state of ^{15}N are describable in terms of single-hole excitations in a doubly closed-shell core. Practical calculations using microscopic theories of nuclear reactions have so far been restricted to such relatively simple structures. For comparison between experimental and theoretical results, therefore, an unambiguous identification of the particle-hole resonances is required, in particular the $d_{\frac{3}{2}}$ single-particle resonances.

Since isospin $T = 0$ is not allowed in n+^{15}N and the density of $T \geqq 2$ states in ^{16}N is negligible in the energy region of interest, one may hope to see the simple $T = 1$ resonances of particle-hole character in a not too dense background of more

complicated excitations. Also below $E_n = 5.65$ MeV, only the elastic channel is open, which considerably simplifies the theoretical analysis.

The motivation for the present experiments was therefore threefold:

(i) To resolve by means of phase-shift and *R*-matrix analyses of the measured cross sections previous discrepancies regarding spin and parity assignments.

(ii) To establish the positions of the $d_{\frac{3}{2}}$ single-particle resonances.

(iii) To extend the measurements to the region of the giant dipole resonance.

In sect. 2, we discuss the measurement and *R*-matrix analysis of the total cross section. In sect. 3, the measurements of the differential cross sections are presented. The results of a phase-shift analysis are described, which yields a determination of the $d_{\frac{3}{2}}$ single-particle resonance energies. In sect. 4 we compare our assignments with the results of previous work. In the paper following this [15]), the present results for differential and total cross sections are compared with those of microscopic coupled channel calculations.

2. Total neutron cross section

2.1. EXPERIMENTAL ARRANGEMENT

The total neutron cross section of ^{15}N has been measured with the time-of-flight spectrometer at the Karlsruhe isochronous cyclotron. The spectrometer consists of a 57 m flight path, a 9 cm diameter by 1 cm thick proton recoil detector and a 20 kHz pulsed neutron source with approximately 1.5 ns burst width. Details of the operation have been given elsewhere [16]).

The ^{15}N data were obtained for the neutron energy range 0.9 to 32 MeV by transmission measurements. Standard time-of-flight methods were used for data collection. The measurements utilized a 45 g sample of ^{15}N in the form of liquid $^{15}NH_3$ in a stainless steel container. The enrichment of ^{15}N was 99.0 %. The chemical impurity other than $^{14}NH_3$ was less than 0.01 %. The sample area was 3.75 cm^2 and the neutron beam was collimated to 1.2 cm by 3 cm at a distance of 1.1 m from the source. Further collimation at 10 m and 37 m limited the solid angle at the detector to $\approx 3 \times 10^{-6}$ sr. An identical empty sample cell was used for the sample-out measurement. The neutron beam was monitored by a γ pulse-shape discriminating detector placed at 6° to the beam at a distance of 11 m from the cyclotron target. Normalization difficulties for sample-in and sample-out measurements were eliminated by automatically alternating the sample in and out of the beam on a 250 sec cycle.

The proton recoil detector consisted of a liquid scintillator NE-213, 9 cm by 1 cm, viewed by an XP-1040 phototube. The average counting rate was 0.8 neutrons per machine burst when the sample was out of the beam. Up to two counts per machine burst could be accepted by the time analyzer, Laben UC-KB, and on-line computer. Corrections for dead-time losses were performed in the data reduction code.

The overall timing resolution achieved in the measurement was 2.7 ns. This value was determined from the observed width of the prompt γ-peak from the cyclotron

target. With the exception of the lowest and highest portions of the spectrum, the counting statistics were better than 2 %.

2.2. DETERMINATION OF THE CROSS SECTION

The total neutron cross section of ^{15}N was calculated by combining sample-in, sample-out and background measurements. The effect of hydrogen in the $^{15}NH_3$ sample was corrected for using recent Karlsruhe measurements and effective range fits of the total neutron cross section for hydrogen [17]). Dead-time corrections were performed using a formula which has been experimentally verified for the condition of two stop-pulses per machine burst. The combined background and dead-time corrections were typically a few percent of the open beam counting rate. At the low-energy end of the spectrum the background reaches about 10 %.

The energy resolution for the measurement was 0.93 keV at 800 keV increasing as $E^{\frac{3}{2}}$ to 240 keV at 32 MeV. The absolute cross-section values are expected to be accurate within 4 %. The total neutron cross section for ^{15}N is shown in figs. 1–5. The representative error bars include only the counting statistics. The experimental energy resolution is indicated by horizontal error bars at several points throughout the range. The solid curves are the results of R-matrix fitting which will be discussed in the next section.

This experimental result has been compared with the neutron data of Fossan *et al.* [5, 6]) and of Sikkema [2]) in the appropriate regions of overlap. Except for resolution effects, the agreement is good. Up to E_n = 11 MeV, 41 resonances were

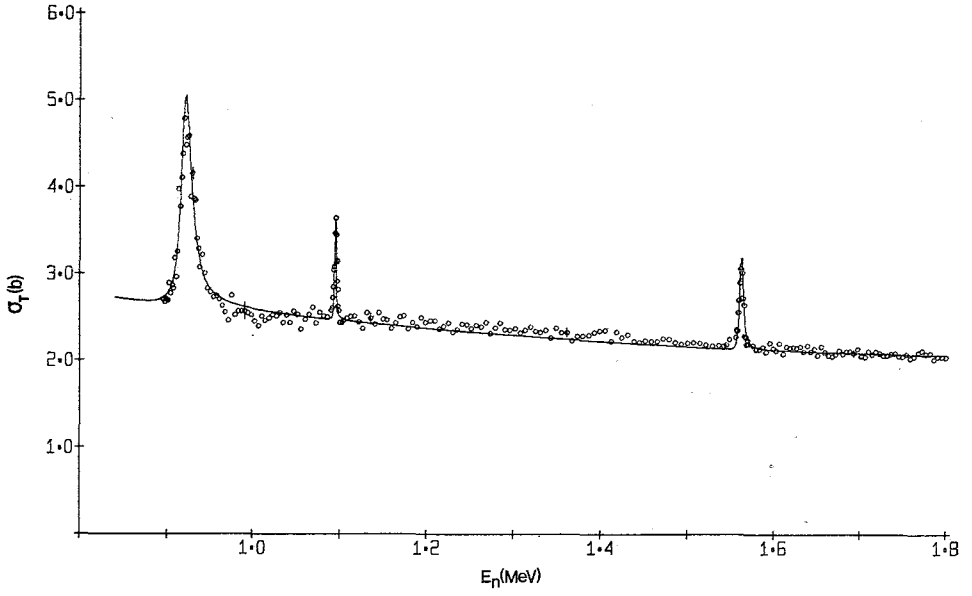

Fig. 1. Total neutron cross section for n+^{15}N from E_n = 0.8–1.8 MeV. The solid line is the result of an R-matrix calculation.

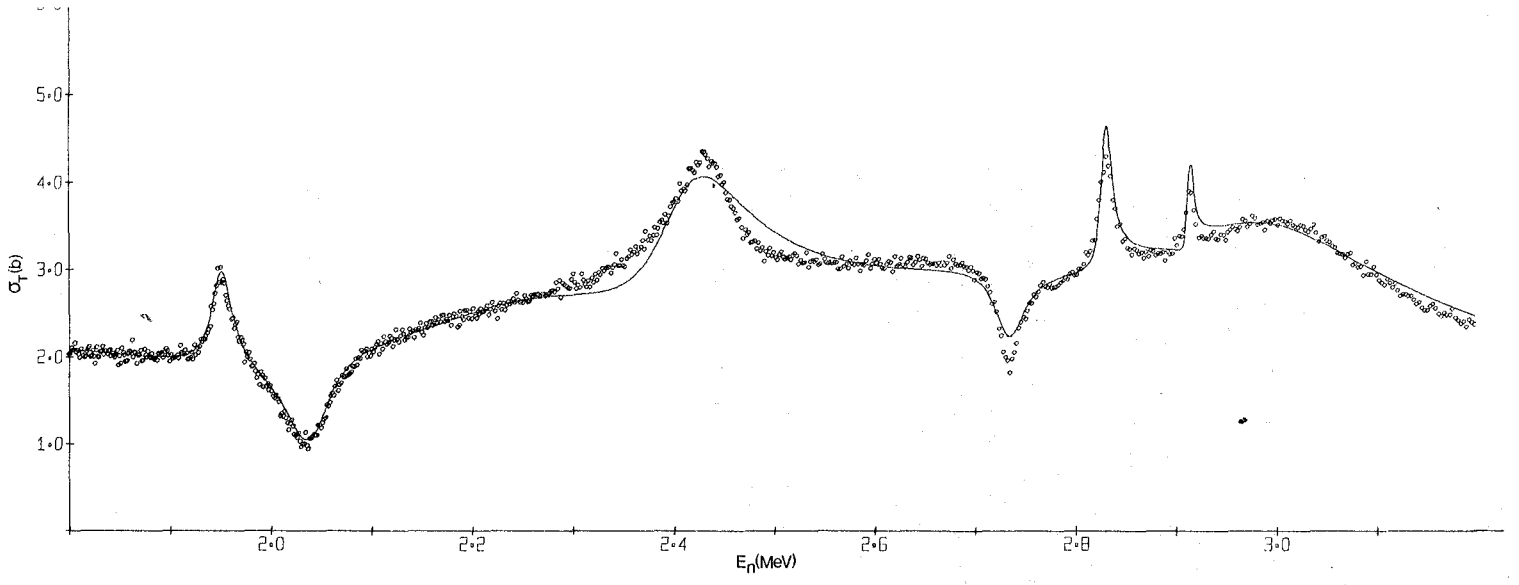
5·0
4·0
3·0
2·0
1·0
σ_T(b)
2·0
2·2
2·4
2·6
2·8
3·0
E_n(MeV)

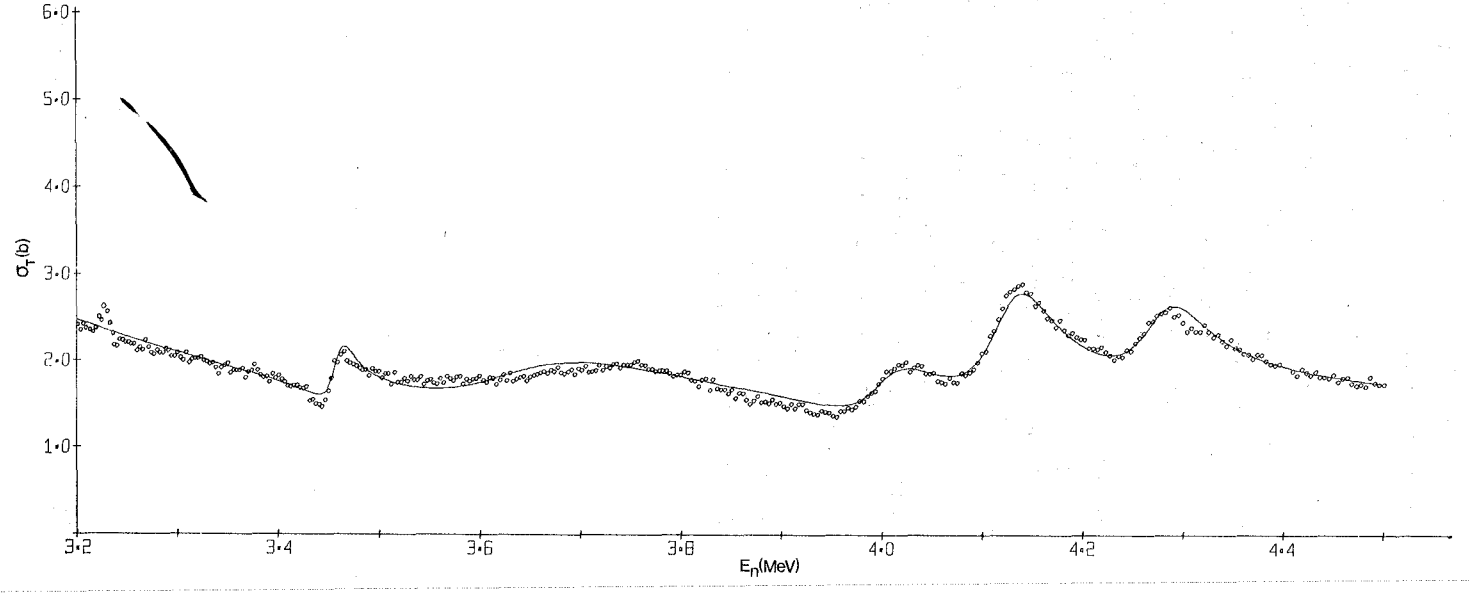
6·0
5·0
4·0
3·0
2·0
1·0
σ_T(b)
3·2
3·4
3·6
3·8
4·0
4·2
4·4
E_n(MeV)

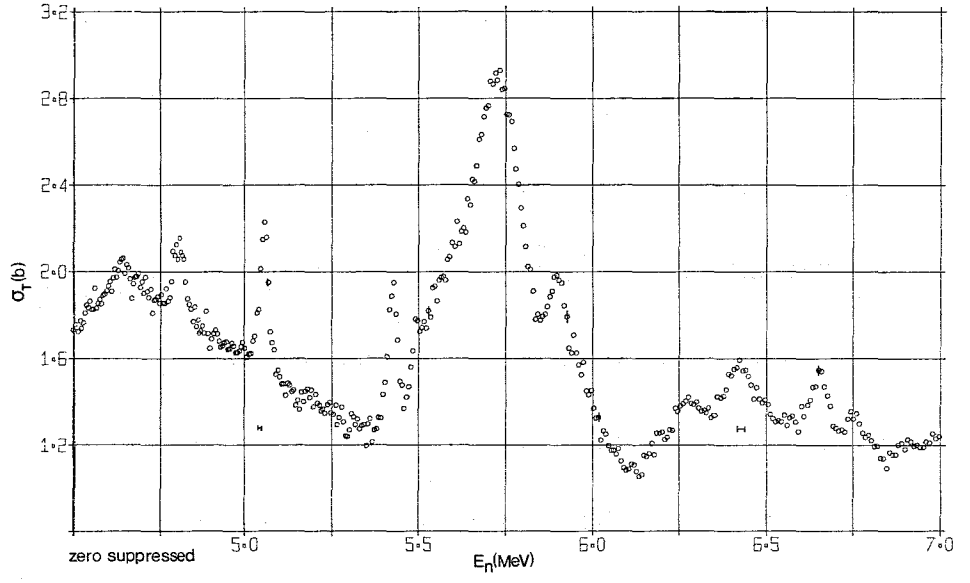

Fig. 3. Total neutron cross section from $E_n = 4.5-7.0$ MeV.

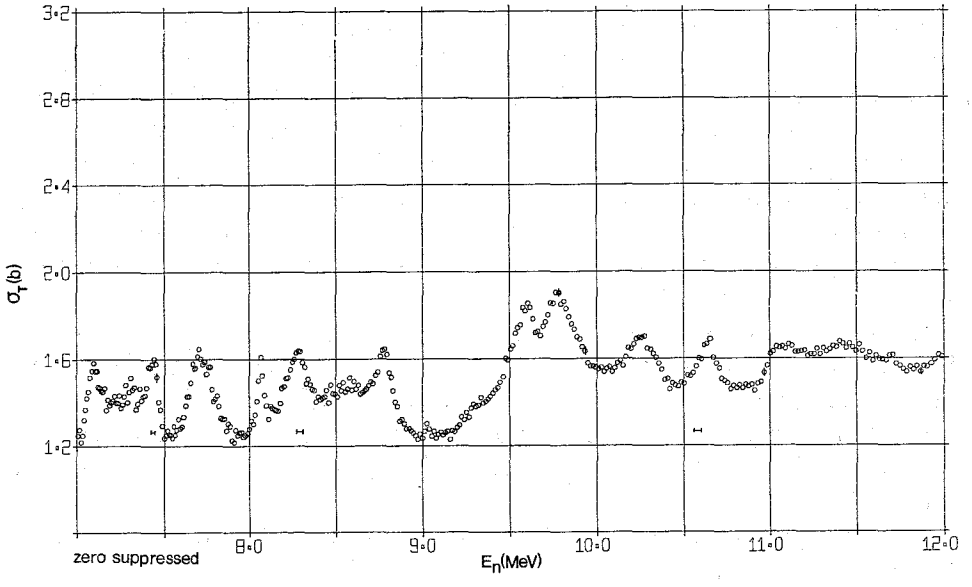

Fig. 4. Total neutron cross section from $E_n = 7.0-12.0$ MeV.

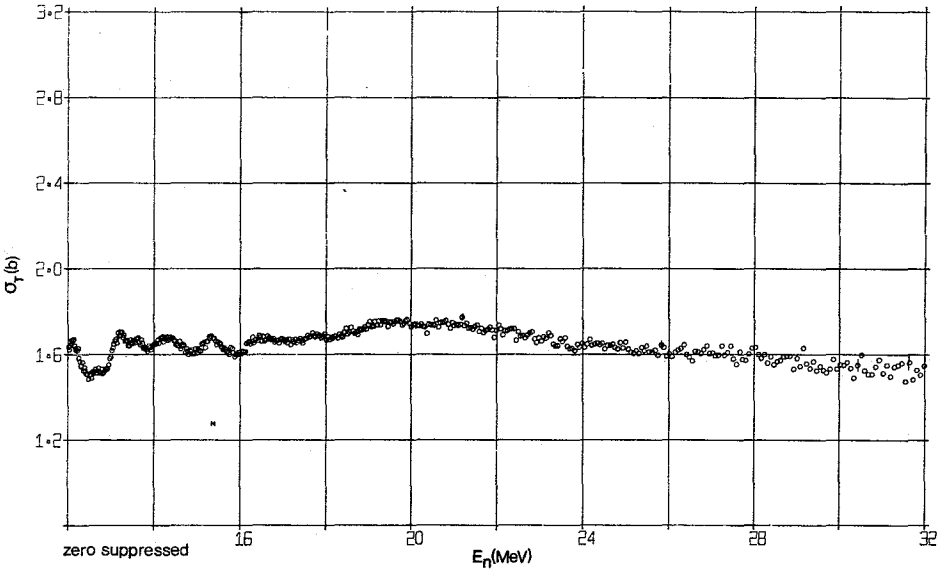

Fig. 5. Total neutron cross section from $E_n = 12.0-32.0$ MeV.

resolved. Above this energy, the cross section shows broad, slowly varying fluctuations.

2.3. *R*-MATRIX ANALYSIS

The total neutron cross section of ^{15}N has been analyzed up to $E_n = 10$ MeV. The analysis has taken two different forms. Below 4.5 MeV, the multilevel *R*-matrix formalism was used to determine E_λ, Γ_λ and whenever possible J^π by a χ^2 fitting and minimization technique. Above this energy, the resonance amplitudes with corrections for experimental resolution were used to infer the *J*-value via the simple $2J+1$ dependence. In this energy range the parity of the resonances cannot be given since no marked interference effects are observed between resonance and potential scattering. Above 5.65 MeV all *J*-values must be understood as lower limits since the inelastic channel is open.

In energy regions where the width of resonances is approaching the spacing, the Breit-Wigner single level formulae are not valid. An appropriate representation below the inelastic threshold is the multilevel *R*-matrix description with a single open channel for elastic scattering. This formalism has been extensively discussed in the literature [18–21]) and the following is intended only as a summary of the formulae used in the present analyis.

With a single open channel, the *R*-matrix is a simple function which is related to the collision matrix U_{lJS} by,

$$U_{lJS} = \exp(-2i\phi_l)\left[1+2iP_l\frac{R_{lJS}}{1-L_lR_{lJS}}\right], \tag{2.1}$$

where ϕ_l represents the hard sphere of background scattering phase and $L_l = S_l + iP_l$ is defined by the logarithmic derivative of the external region wave functions at the channel surface.

Lane and Thomas [20]) suggest a division of the R-matrix into an explicit multilevel sum and a background term R^0_{IJ}.

$$R_{IJ} = R^0_{IJ} + \sum_{\lambda} \gamma^2_{\lambda IJ}/(E_{\lambda IJ} - E). \tag{2.2}$$

The sum extends over the λ levels having orbital momentum l, channel spin S, total angular momentum J and reduced width γ^2_{IJ}: Substitution of eq. (2.2) leaves the form of eq. (2.1) unchanged but the ϕ_l and L_l now include the background term R^0_{IJ}.

For the application of this formalism to resonance analysis, real boundary condition parameters B_l have to be specified. These parameters are closely related to the level

TABLE 1

R-matrix resonance parameters [a]) for ^{15}N+n

E_λ(MeV)	Γ_λ(keV)	J^π	E_λ(MeV)	Γ_λ(keV)	J^π	E_λ(MeV)	Γ_λ(keV)	J^π
0.921	14	1^+ [b])	3.987	88	(1^+)	7.31		
1.095	3	1	4.126	78	(3^-)	7.44	105	$\geqq 2$
1.563	$\leqq 2$	1	4.252	113	(2^+)	7.71	150	$\geqq 2$
1.944	29	1^+ [c])	4.64	> 150	$\geqq 2$	8.07	30	$\geqq 3$
2.038	56	1^- [c])	4.80	37	$\geqq 1$	8.30	175	$\geqq 2$
2.30	412 [d])	1^- [c])	5.055	25	$\geqq 2$	8.77	130	$\geqq 2$
2.399	107	2^+ [c])	5.43	30	$\geqq 3$	9.61		$\geqq 3$
2.732	35	1^-	5.56			9.77		$\geqq 3$
2.830	12	$3(^-)$	5.73	165	$\geqq 4$	10.25		
2.84	714 [d])	2^- [c])	5.90		$\geqq 2$	10.64		
2.915	$\leqq 4$	$\geqq 2$	6.28		$\geqq 1$	11.09		
2.93	260	1^+	6.42		$\geqq 1$	11.41		
3.225			6.65	45	$\geqq 1$	12.10		
3.454	24	1^+	6.76					
3.69	297	1^-	7.10	110	$\geqq 2$			

	$l=0$		$l=1$			$l=2$		
J	0	1	0	1	2	1	2	3
A_{IJ}	0.466 $\times 10^{-1}$	0.394 $\times 10^{-1}$		0.341	228	−0.282	0.484	−0.524 $\times 10^{-1}$
B_{IJ}(keV)$^{-2}$	0.218 $\times 10^{-5}$	0.49 $\times 10^{-5}$		0.14 $\times 10^{-6}$	0.12 $\times 10^{-4}$			
C_{IJ}(keV)$^{-2}$	0.14 $\times 10^{-6}$	0.40 $\times 10^{-7}$			0.14 $\times 10^{-6}$			

[a]) Analysis performed with channel radius $a = 4.69$ fm.
[b]) Parity determined from angular distribution.
[c]) J^π also obtained by phase-shift analysis.
[d]) The uncertainty in the R-matrix results are estimated as $E_\lambda \pm 70$ keV and $\Gamma_\lambda \pm 100$ keV.

shifts $\Delta_{\lambda IJ} = (S_l - B_l)\,\gamma^2_{\lambda IJ}$ and thus are energy dependent via the level shift factor S_l. In this analysis, the level shifts and their energy dependence have been omitted. This procedure corresponds to a special choice of boundary condition parameters $B_l = S_l(E_r)$ where the E_r represent the experimentally observed resonance energies which at resonance coincide with the internal eigenvalues. For s-wave neutrons, where the level shift is identically zero, this procedure is exact and there is no change in interpretation for the usual zero boundary condition.

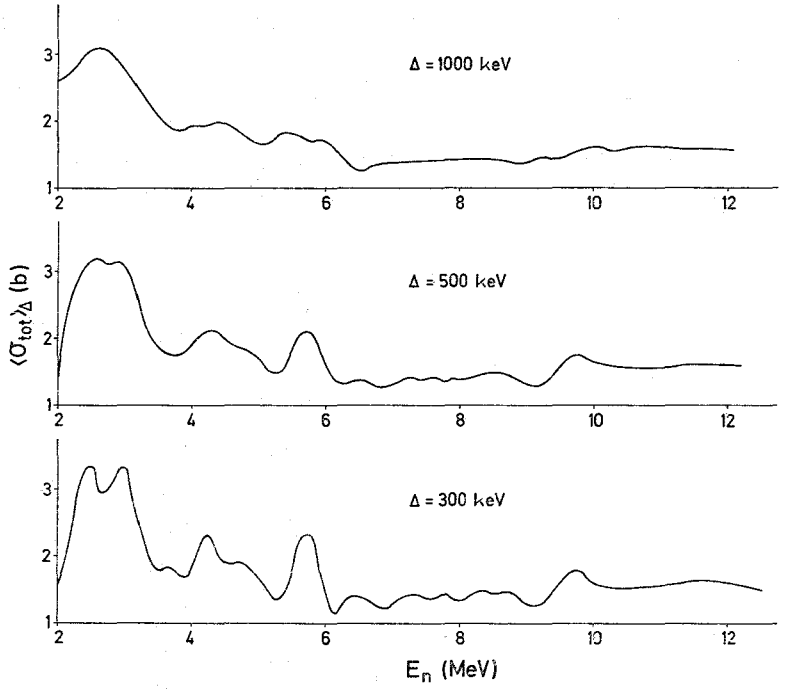

Fig. 6. Energy averaged total neutron cross sections for n+^{15}N. The averaging interval Δ is shown on each curve.

In practical analysis of total neutron cross sections, the parameters E_λ, Γ_λ can be determined only for levels in a restricted energy region. However, the influence of levels outside the region of analysis may not be negligible. This may be accounted for by an expansion of the background term R^0_{IJ} about the median energy E_m of the energy range under consideration [22])

$$R^0_{IJ} = A_{IJ} + B_{IJ}(E - E_m) + C_{IJ}(E - E_m)^2. \tag{2.3}$$

The coefficients A, B and C are l and J dependent in general and represent additional parameters to be determined along with the E_λ and γ^2_λ. The R-matrix program utilizes a χ^2 minimization technique, with a particular set of resonances and their l and J values as input. The results are the parameters E_λ, Γ_λ, A_{IJ}, B_{IJ} and C_{LJ} which best fit the experimental data.

The ^{15}N data up to $E_n = 4.5$ MeV have been fitted and the resonance energies, widths and J-values have been determined. These results together with the A_{lJ}, B_{lJ} and C_{lJ} parameters are given in table 1. The parity can be obtained from total cross-section analyses only when substantial interference occurs, either between resonances or between resonance and potential scattering. Thus for some of the resonances listed in table 1, the parity has not been assigned. In cases where a particular l value is very probable but not certain, the parity is written in parentheses. The total cross section calculated with the parameters of table 1 is shown as the solid line in figs. 1 and 2. In order to obtain maximum self-consistency for the s-, p- and d-wave background phase shifts and the A, B and C coefficients, it is desirable not to subdivide the analysis region into smaller analysis intervals. Thus the entire energy region from 1.8 to 4.5 MeV was fitted with a single-parameter set.

Above 4.5 MeV, no R-matrix analysis was performed. The values E_λ, Γ_λ and J for this region are the observed resonance energy, the width (FWHM) corrected for resolution effects, and the spin inferred from the $2J+1$ rule, respectively.

To facilitate comparison with the p-h calculations of the following paper [15]), it is desirable to eliminate the effects of narrow resonances in the total cross section. To this end, we have calculated the energy-averaged cross section using averaging intervals of 300, 500 and 1000 keV. The results are shown in fig. 6.

3. Differential scattering cross sections

3.1. EXPERIMENTAL ARRANGEMENT

The differential cross sections were measured with a time-of-flight spectrometer using pulsed beam techniques [23]). The measurements were performed in the neutron energy range between $E_n = 0.8$ to $E_n = 3.1$ MeV at the 3 MeV Van de Graaff generator of the University of Hamburg. Neutrons produced by the reactions ^{3}H(p, n)^{3}He (below $E_n = 2.7$ MeV) and ^{12}C(d, n_0)^{13}N (up to $E_n = 3.1$ MeV) were used. The energy spread of the neutrons at 2 MeV was 24 keV for the ^{3}H(p, n)^{3}He and 22 keV for the ^{12}C(d, n_0)^{13}N reaction.

The neutron scattering target consisted of the 45 g of fluid $^{15}NH_3$ already described in the previous section. It was filled in a stainless steel flask of 6.3 cm height, 3.4 cm diameter and 0.5 mm wall thickness. A photomultiplier XP 1040 with liquid scintillator NE 213 of 10 cm diameter and 7.5 cm length served as a detector for the neutrons.

The distance between the neutron source and the neutron target was 30 cm, that between the detector and the scattering sample 105 cm. The scintillator was surrounded by a ring of heavy metal (20 cm length, 10 cm thickness). A cone of heavy metal served as a shadow shielding for both the scintillator and the ring.

The background, mainly produced by the stainless steel flask, was eliminated by automatically alternating once per minute the $^{15}NH_3$ flask and an identical container filled with 0.45 g of $^{14}NH_3$ (corresponding to the 1 % concentration of ^{14}N in the

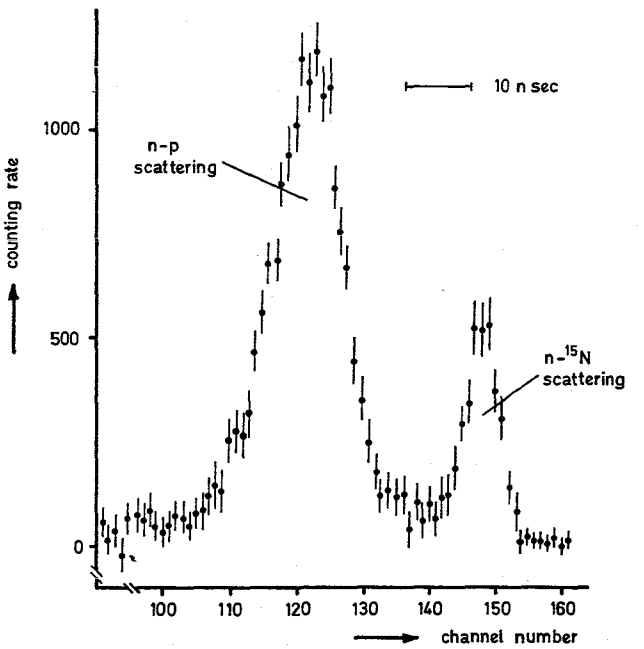

Fig. 7. Neutron time-of-flight spectrum at $\theta_{lab} = 40°$ and $E_n = 2.18$ MeV.

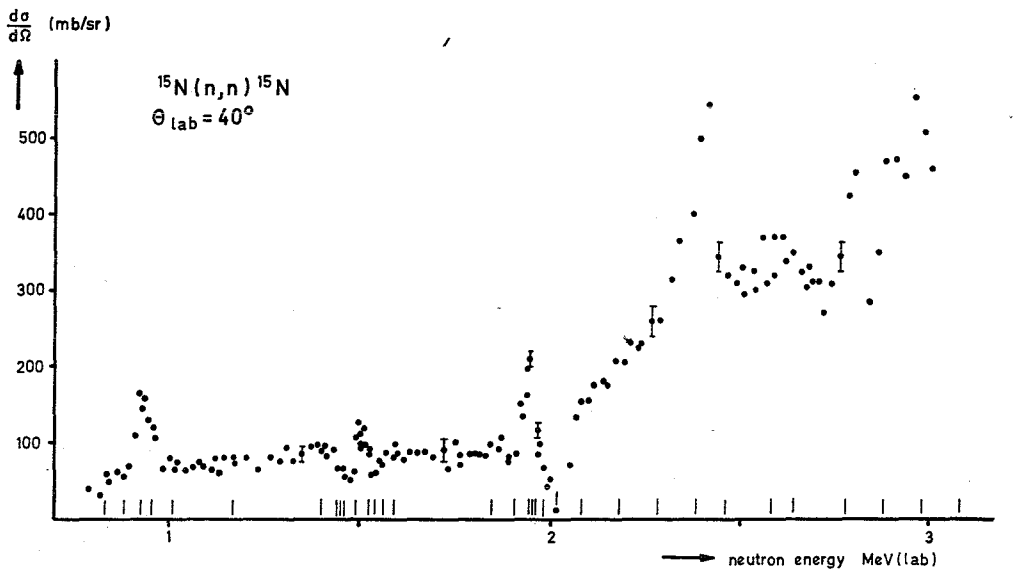

Fig. 8. Excitation function at $\theta_{lab} = 40°$. Angular distributions were measured at the energies indicated by vertical bars.

target). Fig. 7 shows a time-of-flight spectrum taken at $\theta_{lab} = 40°$ and 2.18 MeV neutron energy. The left peak corresponds to the neutrons scattered by the protons of $^{15}NH_3$, the right peak to those scattered by ^{15}N nuclei. From the counting rates of the neutrons scattered by the protons we obtained the normalization for the absolute cross sections. The relative efficiency of the detector as a function of energy was determined by measuring the known ^{3}H(p, n)^{3}He cross sections. For angles smaller than about 60° the n-p counting rates simultaneously served as an additional monitor.

3.2. EXPERIMENTAL RESULTS

In order to determine the level parameters of the broad resonances ($\Gamma > 20$ keV) between $E_n = 0.8$ and $E_n = 3.1$ MeV, we performed measurements of the excitation functions at $\theta_{lab} = 40°$ and $\theta_{lab} = 140°$ and a total of 33 angular distributions. The excitation function at $\theta_{lab} = 40°$ is shown in fig. 8. The positions of the resonances with $\Gamma > 10$ keV at $E_n = 0.93$, 1.56, 1.94, 2.05, 2.4 and 2.7 MeV are in agreement

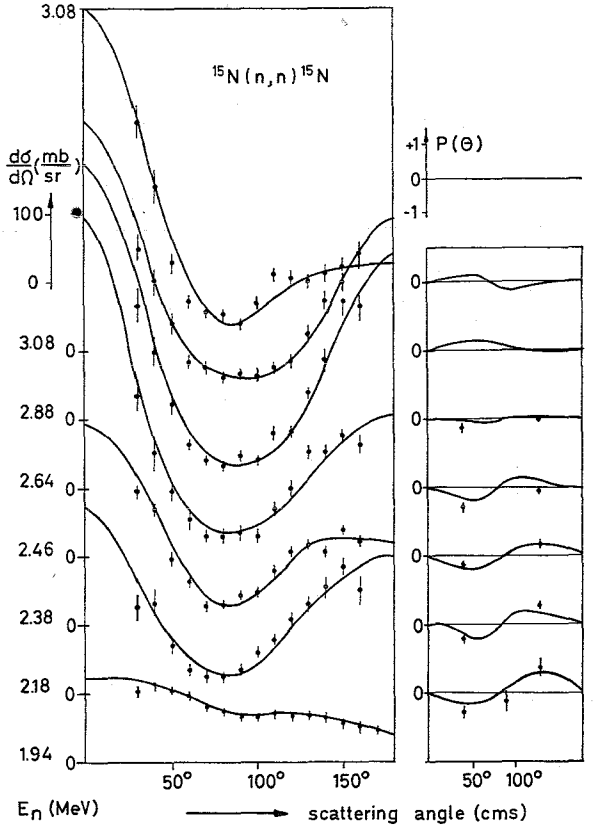

Fig. 9. Some typical angular distribution and polarization data together with fits obtained from phase-shift analysis (solid lines).

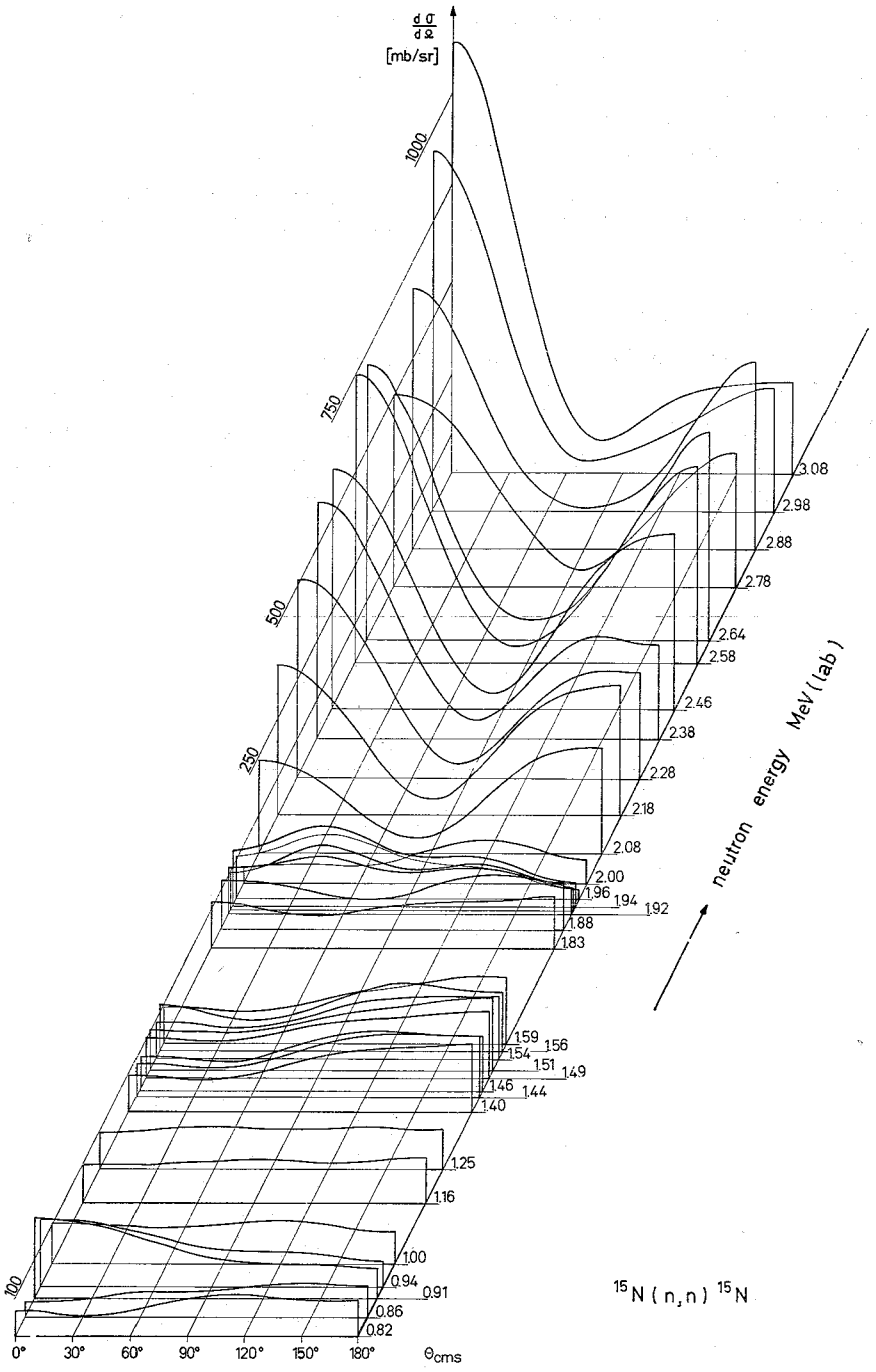

Fig. 10. Differential cross sections for $^{15}N(n, n)^{15}N$ obtained from Legendre polynomial fits to the experimental data.

with the results from the total cross sections (sect. 2), whereas the narrower resonances could not be resolved.

At the energies indicated by vertical bars in fig. 8, measurements of the angular distributions $d\sigma/d\Omega$ were performed. Previous analyses [2, 24]) suggest that the broad overlapping 1^- and 2^- single-particle resonances lie between $E_n = 2-3$ MeV. Therefore the measurements of the angular distributions in this energy region were mainly performed at energies where the influence of the narrow resonances can be assumed to be small.

The angular distributions were measured in steps of about 10°, mostly between $\theta_{c.m.s.} = 30°$ and $\theta_{c.m.s.} = 160°$. Several examples showing the statistical errors typical for all the angular distributions measured are presented in fig. 9. In order to give a compact representation of the measured data, we present in fig. 10 the results of a χ^2 fit including Legendre polynomials up to fourth order. There is an overall agreement with the data of refs. [2, 3]) in the corresponding energy regions (see fig. 6 of part II, ref. [15])).

TABLE 2
Analyzing power of ^{15}N

E_n(MeV)	$P(40°)_{lab}$	$P(130°)_{lab}$
1.94	-0.54 ± 0.17	$+0.73\pm0.27$
2.08	-0.71 ± 0.26	$+1.20\pm0.23$
2.18	-0.42 ± 0.16	$+0.54\pm0.14$
2.38	-0.25 ± 0.08	$+0.34\pm0.12$
2.46	-0.56 ± 0.15	-0.12 ± 0.08
2.64	-0.28 ± 0.15	-0.03 ± 0.08

In addition, to decide between different sets of phase shifts, rough measurements of the analyzing power of ^{15}N were done at scattering angles $\theta_{lab} = 40°$ and $\theta_{lab} = 130°$ in the energy region between $E_n = 1.94$ and $E_n = 2.64$ MeV. The ^{12}C(d, n_0)^{13}N reactions was used [25, 26]) as a source of polarized neutrons at $\theta_{lab} = 20°$. The analyzing power was determined by measuring the left-right counting rate asymmetry. The results are presented in table 2 and fig. 9 together with the statistical errors.

3.3. PHASE-SHIFT ANALYSIS

In order to determine the energies and spin and parity assignments of the broad resonances between $E_n = 1.8$ and 3.1 MeV, a phase-shift analysis was performed. It was based on a parametrization of the scattering matrix by phase shifts δ_{SlJ} where S is the channel spin, l the orbital angular momentum and J the total spin of the compound nucleus state. A method similar to that described by Tombrello [27, 28]) has been employed for the calculations. Phase shifts up to $l = 2$, allowing splitting of the triplet phases, were used. Hard-core phase shifts served as starting parameters for the χ^2 fits. We used a grid search method [29]). For each energy, the experimental

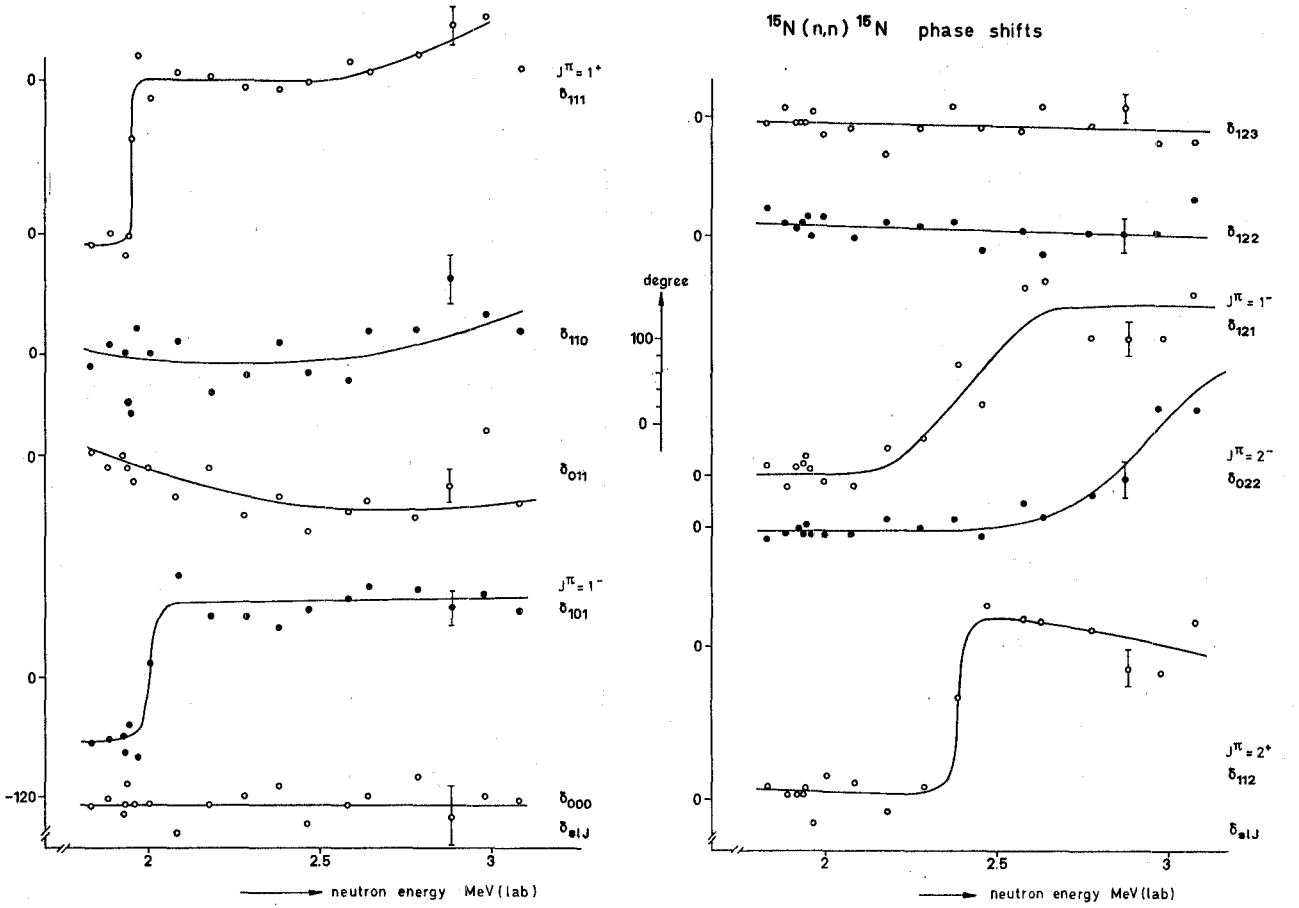

Fig. 11. Results of the phase-shift analysis for the reaction ^{15}N(n, n)^{15}N. The solid lines are freely drawn through the points.

data for the total cross section, the angular distribution and (if measured) the polarization were fitted simultaneously.

In fig. 9 several examples of the fits obtained (solid lines) are shown together with the corresponding experimental values. The phase shifts as a function of energy are presented in fig. 11. At 2.88 MeV, typical error bars are shown which are the standard deviations for the fit, calculated from the variance matrix. The scattering of the points around the freely drawn solid lines may also be due to the influence of the narrow resonances. The phase-shift analysis clearly indicates resonances at 1.94, 2.05, 2.4, 2.42 and 2.94 MeV.

In good agreement with the results of Hewka *et al.* [24]), obtained via the ^{15}N(d, p)^{16}N reaction, the phase-shift analysis indicates broad 1^- and 2^- resonances at $E_n = 2.42 \pm 0.08$ and 2.94 ± 0.1 MeV with approximate widths of $\Gamma = 250 \pm 50$ and 320 ± 80 keV, respectively. These widths were estimated directly from fig. 11, as the energy range over which the phase shift changes from $\delta = \frac{1}{4}\pi$ to $\delta = \frac{3}{4}\pi$, the resonance energy corresponding to $\delta = \frac{1}{2}\pi$. The rise of the δ_{111} and δ_{011} phase shifts near 2.9 MeV may be caused by a broad 1^+ resonance also seen in the total cross section in this energy region.

In the next section we combine the results of the phase-shift analysis with those from the *R*-matrix fits and compare with the assignments of previous work. The total cross sections and the angular distributions in the region of the single-particle resonances are compared with the results of microscopic coupled channel calculations in part II of this paper [15]).

4. Discussion

In this section, a comparison with previous resonance assignments is made, using the results of sects. 2 and 3. The resonances below 4.5 MeV are considered individually (see also table 1).

The 0.921 MeV *resonance.* This resonance is assigned $J = 1^+$, in agreement with refs. [3, 5, 24]). Although the *R*-matrix analysis cannot distinguish with certainty between $l = 1$ and 2 in this energy region, a positive parity assignment seems indicated by the forward peaking of the angular distribution.

The 1.095 MeV *resonance.* A value of $J = 1$ is determined from the total cross section. This results is consistent with the values ($0^-1^-2^-$) given in ref. [24]). We disagree with the assignment of 0^+ suggested in ref. [5]), since the observed peak cross section does not seem to permit a value other than $J = 1$.

The 1.563 MeV *resonance.* Our assignment of $J = 1$ is consistent with that of refs. [5, 24]). The parity could not be determined.

The 1.994 MeV *resonance.* The phase-shift and *R*-matrix analyses are in agreement with the results of refs. [2, 5, 24]), which all give an assignment of 1^+ for this level.

The 2.038 MeV *resonance.* The *R*-matrix and phase-shift results definitely establish the assignment of 1^-, in agreement with refs. [2, 5]).

The 2.30 MeV *resonance.* Both analyses indicate a broad 1^- resonance in the region 2.3 – 2.4 MeV, in agreement with ref. [24]). The overlap of the *R*-matrix and the phase-shift results for the width, $\Gamma \approx 412 \pm 100$ keV and $\Gamma \approx 250 \pm 50$ keV respectively is poor. The phase-shift analysis is complicated by the presence of other resonances in the neighbourhood of the wide 1^- level. The *R*-matrix widths in table 1 are the energy-dependent widths $\Gamma_\lambda(E) = 2P_l(E)\gamma_{\lambda l}^2$ evaluated at the resonance energy E_λ. The observed widths (FWHM) will be somewhat less than these values because of the energy dependence of the shift function [20]) S_l. In addition, the *R*-matrix fit program minimizes $\sum_i(\sigma_{\text{calc}}^i - \sigma_{\text{exp}}^i)^2$. This procedure leads to an increased uncertainty for such a broad resonance. Nevertheless both results are in rough agreement with that from the ^{15}N(d, p)^{16}N reaction obtained by Hewka *et al.* [24]), $\Gamma = 290 \pm 30$ keV.

The 2.40 MeV *resonance.* Both analyses indicate a 2^+ state, consistent with refs. [2, 24]).

The 2.732 MeV *resonance.* The *R*-matrix analysis assigns 1^- to this level. The inverted shape indicates an s-wave resonance. Attempts to obtain an inverted resonance as a d-wave interference with the broad 1^- resonance at 2.30 MeV were unsuccessful.

The 2.830 MeV *resonance.* Analysis of the total cross section indicates $J = 3$. Because of the very small penetrability of $l = 3$ neutrons at this energy, an assignment of 3^- is highly probable. This is consistent with ref. [2]), where $J = (3^-4^-5^-)$ is given.

The 2.84 MeV *resonance.* Both analyses indicate a broad resonance near 2.9 MeV with $J^\pi = 2^-$ in agreement with ref. [24]). As for the broad resonance at 2.30 MeV, the width $\Gamma \approx 320$ keV observed in the phase-shift analysis is considerably less than the *R*-matrix width of $\Gamma \approx 714$ keV.

The 2.915 MeV *resonance.* Due to the narrow width of this resonance, we obtain only $J \geqq 2$.

The 2.93 MeV *resonance.* The *R*-matrix fits to the total cross section require a broad 1^+ state at this energy. This assignment is also suggested by the phase-shift analysis. This disagrees with ref. [2]), where the values $J = 2^+$ or 3^+ are given and with ref. [24]), where no evidence for this level was seen.

The 3.454 MeV *resonance.* The interference shape seen in the total cross section indicates a p-wave resonance. The shape is not consistent with an s-wave resonance at this energy. The *R*-matrix analysis yields $J = 1^+$.

The 3.69 MeV *resonance.* An assignment of 1^- is given to this resonance. As previously noted in ref. [6]), the amplitude of the peak is consistent with either $J = 1$ or 2, but $J = 3$ [ref. [24])] requires an unreasonable low background. An assignment of 2^- is eliminated because the strong minimum predicted by the *R*-matrix near 3.56 MeV due to the interference with the broad 2^- state at 2.84 MeV was not observed. The possibility of 1^+ or 2^+ is ruled out because resonance-potential interference was not seen as in the case of the 1^+ resonance at 3.454 MeV.

The 3.987 *and* 4.252 MeV *resonances.* The shapes of these resonances are consistent with 1^+ and 2^+ assignments respectively. The assignments should be considered

tentative since the resonances between 4.0 and 4.5 MeV are strongly overlapping.

The 4.126 MeV *resonance*. The cross section calculated with 3^- for this level gives good agreement with experiment. However, since our analysis has been limited to s-, p- and d-wave neutrons, the possibility of higher J-values could not be excluded. A broad level near 4.2 MeV underlying the three resonances resolved at 3.987, 4.126 and 4.252 has been reported in refs. [6, 24]) where it was assigned ($J = 3$) and (2^-) respectively. We attempted to include this resonance in our analysis. However, an assignment of $J = 3$ was inconsistent with the R-matrix analysis and a 2^- assignment gave a poor fit and large χ^2. This analysis is complicated by the presence of another wide resonance at 4.64 MeV. But the inclusion of this level in the calculation would only decrease the probability of the existence of a broad state at 4.2 MeV. We thus conclude that only the above three resonances are present in this region.

Above 4.5 MeV only lower limits are given for the resonance spins. These were obtained by estimating a smooth background from potential scattering and applying the $2J+1$ limit to the peak cross sections. The R-matrix analysis was not pursued further since (i) the inelastic channel opens at 5.65 MeV, (ii) the cross section is increasingly complex and a unique set of spins and parities is more difficult to obtain and (iii) the limitation to s-, p- and d-wave neutrons is becoming more dubious.

5. Conclusions

We have presented the results of phase-shift and R-matrix analyses of the total cross section for the reaction ^{15}N(n, n)^{15}N in the energy region up to $E_n = 4.5$ MeV. This analysis has enabled us to resolve some previous ambiguities regarding spins and parities of levels in the compound system ^{16}N. In addition, a number of new levels have been observed above $E_n = 6.5$ MeV, and tentative spin assignments are suggested on the basis of the $(2J+1)$ rule.

The present experiments, plus the R-matrix and phase-shift analyses of the results, have resolved the uncertainty concerning the positions of the broad 1^- and 2^- resonances which are assumed to arise from the $(d_{\frac{3}{2}}\, p_{\frac{1}{2}}^{-1})_{1^-,2^-}$ shell-model configuration. Our energies of $E_n = 2.4$ and 2.9 MeV for the 1^- and 2^- levels, respectively, are in good agreement with the results of Hewka *et al.* [24]). These results are analyzed in terms of a particle-hole coupled channel calculation in the following paper [15]).

The authors gratefully acknowledge the assistance of the cyclotron group at Karlsruhe and the Van de Graaff group at Hamburg, in particular D. Kopsch, L. Kropp and B. Pollermann. Much of the motivation for this work originated in discussions with H. A. Weidenmüller and K. Dietrich. Useful discussions with W. Ebenhöh, W. Glöckle, J. Hüfner and B. Pöpel have provided additional impetus.

References

1) L. Schellenberg, E. Baumgartner, P. Huber and F. Seiler, Helv. Phys. Acta **32** (1959) 337
2) C. P. Sikkema, Nucl. Phys. **32** (1962) 470
3) T. R. Donogue, A. F. Behof and S. E. Darden, Nucl. Phys. **54** (1963) 49
4) T. R. Donogue, R. A. Blue, J. E. Jackson, C. R. Soltesz and K. J. Stout, Bull. Am. Phys. Soc. **9** (1964) 628
5) D. B. Fossan, R. A. Chalmers, L. T. Chase and S. R. Salisbury, Phys. Rev. **135** (1964) 1347
6) D. B. Fossan, R. A. Chalmers, S. R. Salisbury and J. F. Vaughn, Phys. Rev. **152** (1966) 980
7) R. H. Lemmer and C. M. Shakin, Ann. of Phys. **27** (1964) 13
8) V. V. Balashov *et al.*, Sov. J. Nucl. Phys. **2** (1966) 461
9) W. Ebenhöh, W. Glöckle, J. Hüfner and H. A. Weidenmüller, Z. Phys. **202** (1967) 301
10) H. G. Wahsweiler, W. Greiner and M. Danos, Phys. Rev. **170** (1968) 893
11) J. Hüfner and R. H. Lemmer, Phys. Rev. **175** (1968) 1394
12) W. Ebenhöh and B. L. Andersen, Nucl. Phys. **A127** (1969) 209
13) C. B. Dover and P. Sandner, Phys. Lett. **29** (1969) 405
14) B. Pöpel and G. Schütte, Z. Phys. **231** (1970) 48
15) C. B. Dover *et al.*, Nucl. Phys. **A166** (1971) 461
16) S. Cierjacks, B. Duelli, P. Forti, D. Kopsch, L. Kropp, M. Lösel, J. Nebe, H. Schweikert and H. Unseld, Rev. Sci. Instr. **39** (1968) 1279
17) S. Cierjacks, P. Forti, G. J. Kirouac, D. Kopsch, L. Kropp and J. Nebe, Phys. Rev. Lett. **23** (1969) 866
18) E. P. Wigner, Phys. Rev. **70** (1946) 15
19) E. P. Wigner and L. Eisenbud, Phys. Rev. **72** (1947) 29
20) A. M. Lane and R. G. Thomas, Rev. Mod. Phys. **30** (1958) 257
21) J. E. Lynn, Theory of neutron resonance reactions (Clarendon Press, Oxford, 1968)
22) F. W. K. Firk, J. E. Lynn and M. C. Moxon, Proc. Phys. Soc. **82** (1963) 477
23) S. J. Skorka, Nucl. Instr. **28** (1964) 62
24) P. V. Hewka, C. H. Holbrow and R. Middleton, Nucl. Phys. **88** (1966) 561
25) J. R. Sawers, F. O. Purser and R. L. Walter, Phys. Rev. **141** (1966) 825
26) M. M. Meier, L. A. Schaller and R. L. Walter, Phys. Rev. **150** (1966) 821
27) T. A. Tombrello, C. M. Jones, G. C. Phillips and J. L. Weil, Nucl. Phys. **39** (1962) 541
28) T. A. Tombrello, Phys. Rev. **138** (1965) B40
29) F. James and M. Roos, CERN Program Library 67/623/1

2.C: 2.L

Nuclear Physics **A166** (1971) 461—478; © *North-Holland Publishing Co., Amsterdam*

NEUTRON SCATTERING FROM ^{15}N

(II). Coupled channel calculations

C. B. DOVER

Institut für theoretische Physik der Universität
und Max-Planck-Institut für Kernphysik, Heidelberg,

S. CIERJACKS, G. J. KIROUAC and J. NEBE

Institut für Angewandte Kernphysik, Kernforschungszentrum Karlsruhe

and

H. H. DUBENKROPP, R. PUTZKI and B. ZEITNITZ

(II). *Institut für Experimentalphysik der Universität Hamburg*

Received 23 September 1970

Abstract: The total and differential cross sections for the scattering of neutrons from ^{15}N in the energy region $0 \leqq E_n \leqq 12$ MeV are analyzed by the method of coupled channels, in a 1p-1h configuration space. The 1^- and 2^- resonances observed experimentally at $E_n = 2.3$ and 2.9 MeV, respectively, are identified with the $(d_{\frac{3}{2}}\, p_{\frac{1}{2}}^{-1})_{1^-,2^-}$ coupling in the p—h model. The absolute cross sections and angular distributions are in reasonably good agreement with experiment in the region $2 \leqq E_n \leqq 3$ MeV of the $d_{\frac{3}{2}}$ single-particle resonance. Some of the other particle-hole resonances predicted by theory are tentatively identified with broad peaks seen in the *energy-averaged* total cross section.

1. Introduction

In the preceding paper [1]), hereafter referred to as I, the experimental measurement of the total cross section for the n+^{15}N reaction is discussed. A phase-shift and *R*-matrix analysis has also been carried out in I to determine the spins and parities of levels in ^{16}N. In the present paper, we approach the analysis of the observed cross sections from the point of view of a coupled channel calculation [2]).

The coupled channel method provides a way of calculating the properties of compound nuclear resonances in the framework of a microscopic model. In order for the number of channels to be numerically tractable, we restrict our attention to a simple class of compound states, i.e. 1p-1h excitations. Because of this limitation, we do not expect to reproduce in detail all the narrow resonances seen in the experimental cross section. Instead, the emphasis is placed on the *energy-averaged* cross section, in which the effects of the narrow compound resonances have been smoothed out. The p-h model is then invoked to explain the broad resonance structure remaining after a suitable energy average has been performed.

The p-h model has been applied with some success to γ-ray processes involving the

excitation of the giant dipole state in light nuclei [3-10]). The p-h model seems especially appropriate for reactions like $^{16}O(\gamma, n)^{15}O$ for example, since the γ-ray is expected to *selectively* excite mostly 1^- p-h excitations. If ^{16}O is viewed as a doubly closed shell core (which may not be a good assumption), the entrance channel in the above reaction is 0p-0h, and hence the simplest compound state which can be excited after one interaction is a 1p-1h state. In the reaction $^{15}N(n, n')^{15}N$, on the other hand, the entrance channel is already a 1p-1h state in the shell-model description and after one interaction we can excite 2p-2h configurations. Thus in the reaction $n + {}^{15}N$, we no longer expect to excite selectively only the simple 1p-1h compound states. However, one might still expect to find a hierarchy of widths, in which 1p-1h resonances would generally be somewhat broader than more complicated excitations. The existence of such a hierarchy would enable one to isolate the p-h structure by performing an energy average of the cross section.

Since only $T \geqq 1$ states are excited in the reaction $n + {}^{15}N$, the density of compound states is much smaller than in $^{15}N(p, p')^{15}N$, for instance. The level density in ^{16}N is about 4 levels/MeV between $E_n = 1$ and 10 MeV †. This level density is low enough so that the spreading width of 1p-1h states into more complicated excitations is not necessarily large. Thus one might still expect to see compound resonances which are predominantly of 1p-1h character, at least in the energy-averaged cross section.

In sect. 2, the essential approximations which enter into the coupled channel approach are discussed. The determination of the appropriate shell-model single-particle potential is the subject of sect. 3, while the choice of the residual p-h interaction is treated in sect. 4. Sect. 5 is devoted to a detailed comparison of the coupled channel theory with the experimental results of I. A short summary is provided in sect. 6.

2. The coupled equations

The derivation and numerical solution of coupled equations for particle-hole scattering systems have been discussed extensively in the literature [3-5,11-13]). We do not reproduce the details here, but give only the results necessary for our discussion.

If one expands the scattering wave function of the compound system (here ^{16}N) in terms of the fully antisymmetrized states φ_n of the target nucleus, one obtains in general a set of coupled integro-differential equations for the radial wave functions u_n of the continuum particle. The direct numerical solution of these equations has been carried out in ref. [4]). In this paper, as in refs. [3, 5, 11]), we shall solve a somewhat simpler set of coupled differential equations, obtained by making the following approximations:

(i) We use a phenomenological local Saxon-Woods potential (state-dependent) to simulate the non-local Hartree-Fock potential. (ii) We assume that the residual p-h interaction has zero range (see sect. 4). (iii) We neglect overlap integrals of the scat-

† In this paper, the symbol E_n always refers to the lab. energy of the incident neutron, and Γ to the lab. width of a resonance.

tering solutions $u_n(r)$ with the single-particle states below the Fermi sea. Under these assumptions, we obtain [3-5]) the following set of coupled Schrödinger equations for the radial wave functions $u_\alpha^{J^\pi}(r)$ of the incident particle:

$$\left\{\frac{d^2}{dr^2}+\frac{2\mu}{\hbar^2}(E_{c.m.}-\varepsilon_\alpha-V_\alpha(r))-\frac{l_\alpha(l_\alpha+1)}{r^2}\right\}u_\alpha^{J^\pi}(r)=\frac{2\mu}{\hbar^2}\sum_\beta V_{\alpha\beta}(r)u_\beta^{J^\pi}(r). \qquad (1)$$

The index α or β labels the quantum numbers of a p-h pair coupled to total angular momentum J and parity π. We use the j-j coupling scheme. The specification of the particle and hole orbital angular momenta l_p and l_h and total angular momenta j_p and j_h is included in the index α. Since we restrict our attention to the reaction ^{15}N(n, n')^{15}N*, we always have total isospin $T = 1$, and hence isospin indices are omitted. Further, μ is the reduced mass of the incident nucleon, $E_{c.m.}$ is the incident particle energy in the c.m. system, ε_α is the c.m. excitation energy of the target, and $V_\alpha(r)$ is the central Saxon-Woods potential, which is allowed to depend on the orbital angular momentum l_α of the incident particle. Finally, $V_{\alpha\beta}(r)$ is the p-h coupling matrix element, which is a product of a geometrical factor and the radial wave functions of the hole states in channels α and β. The reader is referred to the paper of Buck and Hill [3]) for details †.

The coupled eqs. (1) were solved numerically by using a slightly modified version of the program REACT-1, which was previously applied to the solution of the coupled Lane equations [13]). In contrast to refs. [3-5]), which restrict attention to the $J^\pi = 1^-$ channel relevant for dipole radiative capture, the calculation of cross sections for ^{15}N(n, n')^{15}N* requires the solution of eq. (1) for all possible J^π combinations.

3. Choice of the shell-model potential and the configuration space

In this work, we restrict the space of ^{15}N target states to include only the $\frac{1}{2}^-$ ground state and the $\frac{3}{2}^-$ third excited state at 6.33 MeV. In the framework of the shell model, we describe these states as pure $1p_{\frac{1}{2}}^{-1}$ and $1p_{\frac{3}{2}}^{-1}$ hole states, respectively, in the doubly closed shell ^{16}O core. Of course, such a description is oversimplified. In particular, we neglect the possibility of ground state correlations in the ^{16}O core. The neglect of correlations is dubious, since simple model calculations (in random phase approximation) indicate appreciable polarization of the ^{16}O core [14]). The description of the $\frac{3}{2}^-$ state as a relatively pure $1p_{\frac{3}{2}}^{-1}$ hole state has also recently been questioned [15]).

In addition to assuming pure shell-model configurations for the $\frac{1}{2}^-$ and $\frac{3}{2}^-$ states of ^{15}N, we also neglect the first two excited states of ^{15}N ($\frac{5}{2}^+$ at 5.28 MeV and $\frac{1}{2}^+$ at 5.30 MeV). These states are presumably of 2h-1p character, and would lead to 2p-2h or more complicated states of the compound system ^{16}N. Since most of the resonances observed in ^{15}N(n, n)^{15}N are probably of 2p-2h (or more complicated) nature, as indicated in sect. 5, the neglect of the $\frac{5}{2}^+$ and $\frac{1}{2}^+$ states in ^{15}N, as well as

† Our eq. (1) is the same as eq. (50) of Buck and Hill, the matrix element $V_{\alpha\beta}(r)$ being defined by eq. (51).

all 2p-2h compound states, is probably the main shortcoming of our calculation.

To generate the shell-model wave functions for the $p_{\frac{1}{2}}^{-1}$ and $p_{\frac{3}{2}}^{-1}$ proton-hole states, we have used a central Saxon-Woods potential with spin-orbit coupling:

$$V_{lj}(r) = -V_{lj}^{(0)} f(r) + V_{lj}^{\text{s.o.}} \left(\frac{\hbar}{m_\pi c}\right)^2 \frac{1}{r}\frac{\mathrm{d}}{\mathrm{d}r} f(r) \boldsymbol{l}\cdot\boldsymbol{\sigma}, \tag{2}$$

where $\hbar/m_\pi c$ is the pion Compton wavelength and

$$f(r) = \left[1+\exp\left(\frac{r-R}{a}\right)\right]^{-1}. \tag{3}$$

Here $R = (A-1)^{\frac{1}{3}} r_0$ is the radius and a the diffuseness of the potential well ($A = 16$). In this work, we have used the values $R = 3.08$ fm and $a = 0.53$ fm. The values of $V^{(0)}$ and $V^{\text{s.o.}}$ necessary to fit the binding energies of the $1p_{\frac{1}{2}}^{-1}$ and $1p_{\frac{3}{2}}^{-1}$ states at their experimental values of 12.11 and 18.44 MeV, respectively, are $V^{(0)} = 52.5$ MeV and $V^{\text{s.o.}} = 9.88$ MeV.

It should be noted that the potential parameters given above are used only in calculating the wave functions for the $p_{\frac{1}{2}}^{-1}$ and $p_{\frac{3}{2}}^{-1}$ proton hole states, which are in turn used only in the calculation of the coupling matrix element $V_{\alpha\beta}(r)$ of eq. (1). The potential parameters which describe the p-wave scattering of the incident neutron, and enter in the potential $V_\alpha(r)$ of eq. (1), are adjusted *independently*.

For the incident neutron, we have also used a Saxon-Woods potential of form (2). In most of the calculations reported here, we have restricted our attention to s-, p- and d-waves. In the absence of a single-particle resonance in the f-wave, this should be adequate below about 8–9 MeV. To fit the potential parameters for s- and d-waves, we fit the experimentally observed [16]) binding energies -4.14, -3.27, $+0.94$ MeV for the $1d_{\frac{5}{2}}$, $2s_{\frac{1}{2}}$ and $1d_{\frac{3}{2}}$ states, respectively, in ^{17}O.

A value $V^{\text{s.o.}} = 5.24$ MeV was required to reproduce the $d_{\frac{3}{2}}$-$d_{\frac{5}{2}}$ spin-orbit splitting. This spin-orbit strength has been subsequently used for all partial waves in the continuum. The resulting values of $V^{(0)}$ are listed as "potential A" in table 1. Potential A corresponds to that used in a previous work [12]). The $d_{\frac{3}{2}}$ state is actually a narrow single-particle resonance with a width of about 90 keV. Potential A reproduces this width as well as the position of the resonance.

The energies of the $2s_{\frac{1}{2}}$, $1d_{\frac{3}{2}}$ and $1d_{\frac{5}{2}}$ states in ^{17}O are well established, while the distribution of the 2p and 1f single-particle strength is subject to considerable doubt. In a study of the positive parity levels of ^{16}O, Eisenberg *et al.* [17,18]) have used $1f_{\frac{7}{2}}$, $2p_{\frac{3}{2}}$, $2p_{\frac{1}{2}}$ and $1f_{\frac{5}{2}}$ single-particle energies (c.m.) of 1.55, 3.57, 5.58 and 7.74 MeV, respectively, with respect to the n+^{16}O threshold. To examine the possibility of *positive* parity resonances in the 1p-1h model (see subsect. 5.3), we have also performed calculations in which the $l = 3$ well depth is adjusted in order to obtain a $1f_{\frac{7}{2}}$ single-particle resonance at 1.55 MeV, as in ref. [17]). A spin-orbit strength $V^{\text{s.o.}} = 5.24$ MeV was used as in potential A. The resulting parameters are listed as

potential B in table 1. This choice of $1f_{\frac{7}{2}}$ resonance energy requires a well depth $\approx$ 20 MeV deeper than other partial waves, which is somewhat unreasonable. If we use the same f-wave well depth as for the d-wave, the $1f_{\frac{7}{2}}$ resonance lies at $\approx$ 8 MeV and is very wide. With potential B, the $1f_{\frac{7}{2}}$ resonance has a width $\Gamma \approx 18$ keV. To obtain the experimental width [16]) $\Gamma \leqq 7$ keV, we would have to make the potential radius R somewhat smaller, and the potential even deeper than in table 1. The above considerations suggest that the $\frac{7}{2}^-$ state at 5.697 MeV in ^{17}O only contains some fraction of the $1f_{\frac{7}{2}}$ single-particle strength.

TABLE 1
Woods-Saxon potential parameters

Potential	Central depth $V^{(0)}$				
	$l=0$	$l=1$	$l=2$	$l=3$	$l=4$
A	57.0	52.5	55.2		
B	57.0	52.5	55.2	76.07	
C	57.0	52.5	55.2	71.15	
D	57.0	52.5	55.2	71.15	55.0

We have also adjusted the $l = 3$ well depth so that the 4^+ resonance resulting from the $(f_{\frac{7}{2}}\, p_{\frac{1}{2}}^{-1})$ coupling lies at the energy $E_n = 5.73$ MeV, which corresponds to a prominent resonance of high spin observed experimentally [1]). The resulting parameters are listed as potential C in table 1. Again, $V^{s.o.} = 5.24$ MeV was used. For potential C, the unperturbed $f_{\frac{7}{2}}$ resonance appeared at $E_n = 3.73$ MeV with a width of $\Gamma \approx 240$ keV.

It has been suggested [19]) that the $(1d_{\frac{5}{2}}\, 1p_{\frac{3}{2}}^{-1})_{4^-}$ configuration can perhaps be identified with a resonance seen experimentally at $E_n \approx 5.42$ MeV in the n+^{15}N reaction. To investigate this possibility within our framework, we have also performed calculations including the g-wave, since this is the lowest partial wave which will endow the 4^- state with a width. The spin-orbit strength was again fixed at $V^{s.o.} = 5.24$ MeV for all partial waves. The depth parameters $V^{(0)}$ are listed as potential D in table 1. For all of the present calculations, we have used a real optical potential without absorption. This is reasonable for the compound system ^{16}N, since the first inelastic channel opens at $E_n = 5.65$ MeV. We have also omitted the absorption above $E_n \approx 5.65$ MeV, since none of the narrow resonances in our calculation (which are primarily affected by the absorption) lie in this energy region.

4. Residual interaction

For the calculation of the p-h matrix elements $V_{\alpha\beta}$ of eq. (1) we assume a zero-range spin-dependent particle-particle interaction of the form

$$V(\boldsymbol{r}_1, \boldsymbol{r}_2) = -V_0(1+g\boldsymbol{\sigma}_1 \cdot \boldsymbol{\sigma}_2)\delta(\boldsymbol{r}_1-\boldsymbol{r}_2). \tag{4}$$

In previous work involving the n+^{15}N reaction [12,20–24]), the parameters $V_0 = 504$ MeV · fm^3 and $g = 0.156$ (Soper mixture) have always been used. These parameters were originally obtained by Brown *et al.* [8]) by requiring that the sum of the 1^- energy eigenvalues for ^{16}O be the same as that of Elliott and Flowers [7]), who used a finite

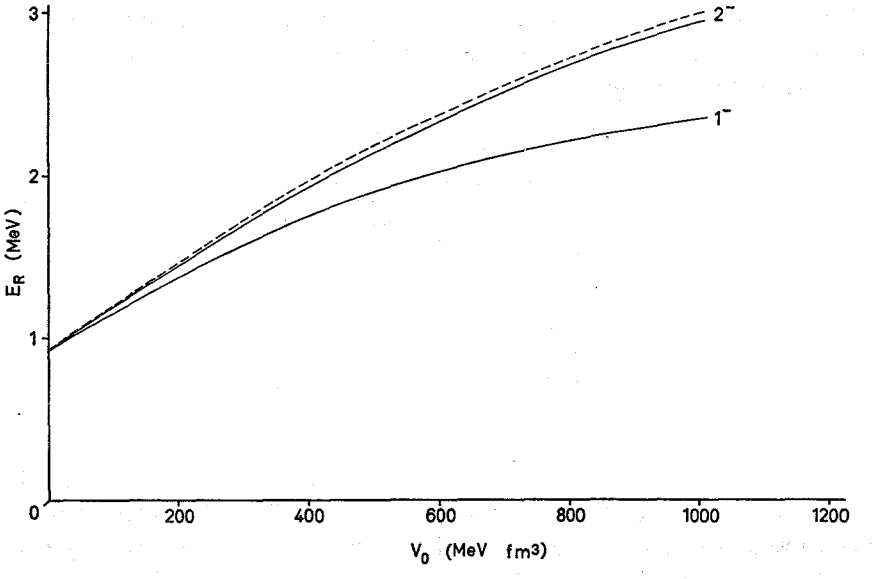

Fig. 1. Resonance energies E_R of the 1^- and 2^- single-particle resonances as a function of the coupling strength V_0 of the residual interaction. The solid lines correspond to a spin mixture $g = 0.156$ while the dashed line refers to $g = 0.312$.

range Yukawa force. This prescription gave reasonable agreement with the energies of the bound states of ^{16}N and the main components of the giant dipole resonance.

We adopt a somewhat different philosophy. We choose V_0 and g such that the energies of the 1^- and 2^- resonances arising from the coupling $(d_{\frac{3}{2}}\, p_{\frac{1}{2}}^{-1})$ lie at $E_n = 2.3$ and 2.9 MeV, respectively. As has been established by the phase-shift analysis of I, the wide resonances observed experimentally close to the above energies involve the coupling of the d-wave to the $p_{\frac{1}{2}}^{-1}$ target ground state. Since we are analysing a scattering experiment, it seems most reasonable to adjust the *effective* force (4) in order to reproduce the dominant features of the cross section rather than bound state information.

The dependence of the 1^- and 2^- resonance energies on the parameters V_0 and g is illustrated in fig. 1. An increase in V_0 moves the resonances to higher energy, increases the 1^-, 2^- energy difference, and decreases the peak cross sections at resonance. The old force parameters [20–24]) yield the 1^- and 2^- resonances at too low an energy with too small a splitting. Since the 1^- energy is independent of g, we first adjust V_0 to locate the 1^- state at $E_n \approx 2.3$ MeV. We then adjust g to get the correct 1^-, 2^- splitting. This prescription gives in principle a *unique* determination of V_0

and g. We find

$$V_0 = 925 \text{ MeV} \cdot \text{fm}^3,$$
$$g = 0.312. \quad (5)$$

It should be remarked that the determination of g is not very accurate, since increasing g from 0.156 to 0.312 only produces a shift of $\approx$ 60 keV in the 2^- resonance. Since the 1^- and 2^- resonances are fairly wide, the phase-shift analysis does not determine their positions to better than about 50 keV.

All calculations in this paper have been done with the parameters V_0, g of eq. (5), or with the choice $V_0 = 970$ MeV · fm^3, which yields essentially equivalent results.

Since the force strength V_0 of eq. (5) is about 85 % stronger than the old value [refs. [20-24])], one must inquire whether the agreement with the bound state energies and the principle dipole state components has been appreciably disturbed. In ref. [21]), the ^{16}N bound state energies (except for the first excited state (0^-)) obtained are consistently too low. In particular, the ground state lies at -2.95 MeV in ref. [21]) and -3.0 MeV in ref. [20]), while the experimental value is -2.5 MeV (with respect to the n+^{15}N threshold). In the coupled channel approach, one does not calculate the bound state energies, so no detailed statement can be made. However, an increase of V_0 *raises* † the energies of all resonant and bound states and hence is in the right direction for removing the above discrepancy with experiment. As shown in sect. 5, the 1^- resonance corresponding to the unperturbed $(d_{\frac{5}{2}}\, p_{\frac{1}{2}}^{-1})_1$ - coupling lies at $E_n \approx 7.75$ in the n+^{15}N reaction. When corrections are made for Coulomb effects ††, this resonance corresponds to an energy of 22.1 MeV in ^{16}O. Various other calculations [refs. [6-8,20-21,30-32])] give values ranging from 21.1 to 22.7 MeV for this state. The experimental [9]) position of the principal component of the giant dipole resonance is $\approx$ 22.3 MeV. The rather small variation in the calculated results does not seem to provide one with a sufficient basis for preferring the old values of V_0 and g to those of eq. (5).

5. Comparison with experimental results

5.1. TOTAL CROSS SECTIONS

In this section, we restrict our attention to calculations employing potential A of table 1 for the continuum and the parameters V_0, g of eq. (5). The total elastic cross section obtained by solving the coupled equations of eq. (1) is shown from 0–12 MeV

† The p-h interaction is repulsive in the $T = 1$ channel, and its diagonal element in eq.(1) makes the effective central potential shallower, thus *increasing* the energies of the bound and resonant p-h states.

†† To compare with levels in ^{16}O, we use $E_{\text{c.m.}}(^{16}\text{O}) = (15/16)E_n + 14.82$ MeV. The 1^- level at $E_n = 2.30$ MeV in n+^{15}N then corresponds to the same energy as the 1^- resonance observed at $E = 17.0$ MeV in ^{16}O$(\gamma, n)^{15}$O. Both levels are attributed to the $(d_{\frac{5}{2}}\, p_{\frac{1}{2}}^{-1})_1$ - coupling. In ref. [20]), a shift of 15.46 is used in the above formula. The difference is not important for our considerations.

in fig. 2, along with the corresponding partial cross sections for the 1^- channel. From this partial cross section and the corresponding ones for other J^π combinations, we extract the resonance energies and widths. These results are tabulated in table 2. It should be noted that the widths given in table 2 are only estimates, and are not the results of a fit to the partial cross sections. The 0^-, 1^- and 3^- resonances expected

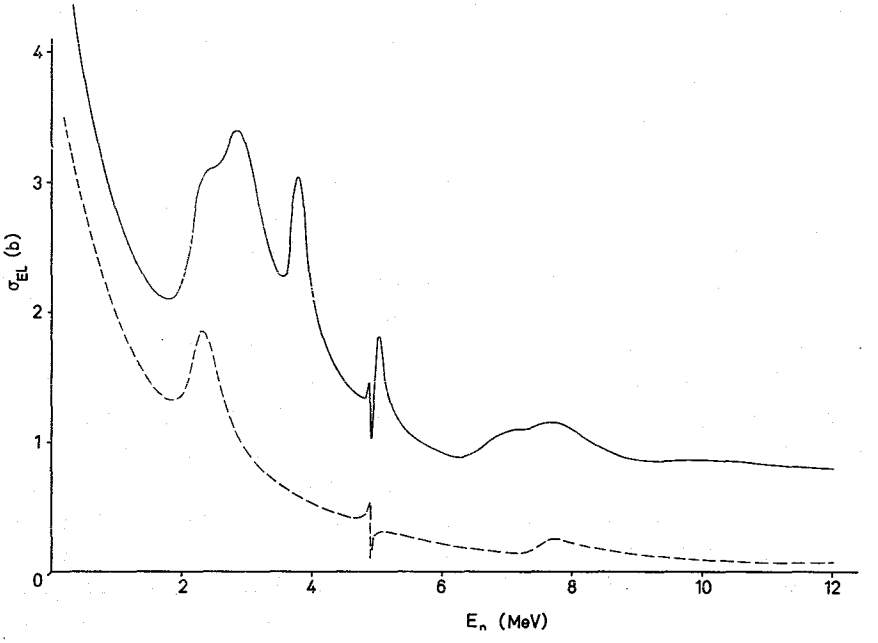

Fig. 2. Total elastic cross section for $n+^{15}N$ (solid line) and corresponding 1^- partial cross section (dashed line) as a function of neutron lab. energy E_n. These calculations were performed with $V_0 = 925$ MeV · fm^3 and $g = 0.312$, using potential A (s, p and d-waves only).

TABLE 2

Calculated resonance energies and widths for $n+^{15}N$

Unpert. conf.	J	$E_n^{unpert.}$	E_n	E_{exc}	Γ
$d_{\frac{3}{2}}\, p_{\frac{1}{2}}^{-1}$	1^-	0.99 MeV	2.3 MeV	16.97 MeV	460 keV
$d_{\frac{3}{2}}\, p_{\frac{1}{2}}^{-1}$	2^-	0.99	2.9	17.54	720
$d_{\frac{5}{2}}\, p_{\frac{3}{2}}^{-1}$	3^-	2.34	3.76	18.34	210
$2s_{\frac{1}{2}}\, p_{\frac{3}{2}}^{-1}$	1^-	3.27	4.89	19.40	80
$d_{\frac{5}{2}}\, p_{\frac{3}{2}}^{-1}$	2^-	2.34	5.02	19.52	120
$2s_{\frac{1}{2}}\, p_{\frac{3}{2}}^{-1}$	2^-	3.27	7.3	21.72	1200–1400
$d_{\frac{5}{2}}\, p_{\frac{3}{2}}^{-1}$	1^-	2.34	7.75	22.06	800–850
$d_{\frac{3}{2}}\, p_{\frac{3}{2}}^{-1}$	2^-	7.74	10.25	24.42	2–3 MeV

Notation as follows: $E_n^{unpert.}$ = unperturbed lab. energy in MeV; E_n = lab. resonance energy (MeV); E_{exc} = excitation energy (c.m.) relative to ground state of ^{16}O; Γ = estimated width (lab.) obtained from partial cross sections for each J^π.

from the $d_{\frac{3}{2}}\, p_{\frac{1}{2}}^{-1}$ coupling are washed out on fig. 2, because of the increased force strength.

The first point to note is that the lowest 1^- and 2^- resonances, corresponding to the $d_{\frac{3}{2}}\, p_{\frac{1}{2}}^{-1}$ unperturbed configuration, have widths of 460 and 720 keV, respectively, which are close to the results obtained from the phase-shift and R-matrix analyses of I.

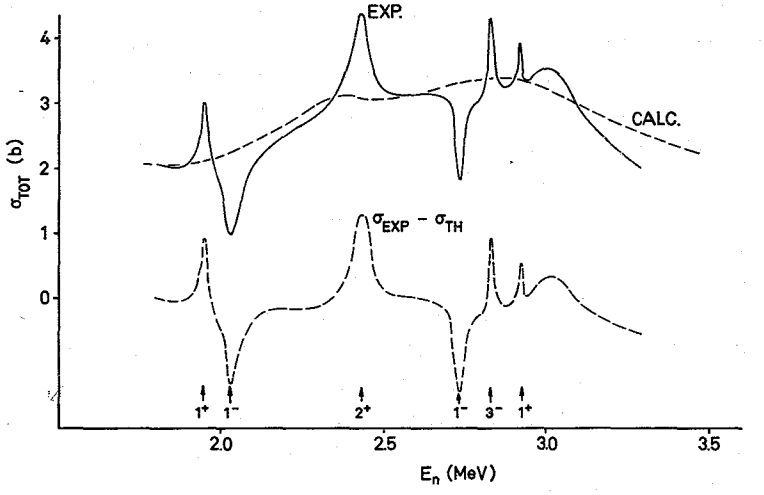

Fig. 3. Total cross section for n+^{15}N in the region of the $d_{\frac{3}{2}}$ single-particle resonance. The solid curve corresponds to the experimental results given in I. The upper dashed curve is the result of a calculation using $V_0 = 925$ MeV · fm^3, $g = 0.312$, and potential A. The lower dashed curve represents the difference of the experimental and calculated cross sections. The resonances are labelled with the spins and parities suggested by the R-matrix analysis of I.

This supports the interpretation of these states in terms of a $d_{\frac{3}{2}}$ single-particle resonance (SPR) shifted upward by the residual p-h interaction. Equivalently, the calculated 1^- and 2^- widths are essentially those characteristic of a d-wave resonance at the appropriate energy in a potential well.

In the experimental results [1]), one sees a number of small resonances in the region 1.9–3.5 MeV superposed on the much wider 1^- and 2^- resonances. These narrow resonances are not predicted by the p-h model. They are presumably of 2p-2h or more complicated character. However, when these narrow resonances are averaged out, the average cross section is very well reproduced by the p-h model in both absolute magnitude and shape between $E_n \approx 1.2$ and 3.1 MeV. This fact further solidifies our interpretation of the dominant reaction mechanism in this region as a d-wave single-particle resonance. This fact is illustrated in fig. 3 which compares experimental and theoretical results in the region of the $d_{\frac{3}{2}}$ resonance. The difference curve $\sigma_{exp} - \sigma_{th}$ between the experimental and theoretical cross sections is almost entirely interpretable as the effect of the small resonances.

It is tempting to try to identify some of the other experimentally observed [refs.

nos. [1,19,25-28])] resonances with calculated p-h resonances. This identification is rather speculative, since no phase-shift or *R*-matrix analysis has been attempted above $E_n \approx 4.5$ MeV and hence the spins and parities of the resonances seen experimentally are not known.

Before launching into a detailed comparison of experiment and theory, we first discuss what one a priori expects to see in the $n+{}^{15}N$ reaction. There are two extreme situations imaginable: (i) One observes strongly excited p-h resonances with widths considerably greater than the surrounding narrow 2p-2h resonances. In this picture, one imagines a hierarchy of compound nucleus states of various degrees of complexity (np-nh), in which states of different complexity do not appreciably mix with each other. Equivalently, the p-h states would have a small spreading width [29]) and hence should be seen as relatively pure p-h resonances in $n+{}^{15}N$; (ii) The strength of the resonances calculated in the p-h model is fragmented due to the mixing of the p-h states with the 2p-2h "doorway" states [29]).

For the $(d_{\frac{5}{2}}\, p_{\frac{1}{2}}^{-1})_{1^-,2^-}$ single-particle resonance configurations discussed above, case (i) seems to apply. Aside from narrow resonances of mostly different spin or parity superposed on top of them, these resonances are well described by the p-h model without fragmentation of their strength. This is understandable, since these excitations lie at relatively low energies (4.65, 5.22 MeV for 1^-, 2^- respectively) in the compound system, where the density of complicated states of the same spin and parity is expected to be small.

For the resonances predicted by the p-h model above $E_n = 3$ MeV the situation is much less clear. Above $E_n = 4.5$ MeV, no *R*-matrix analysis has been performed, and hence our knowledge of the spins of the observed resonances [1]) is restricted to lower limits based on the maximum allowed fluctuation $\Delta\sigma = 0.74\ (2J+1)/E_n$ in the cross section. No information concerning the parities of these levels is available. In view of these facts, the following comments on the possible identification of p-h resonances are necessarily somewhat speculative.

We now consider each of the calculated p-h resonances in turn:

5.1.1. *The* $(d_{\frac{5}{2}}\, p_{\frac{3}{2}}^{-1})_{3^-}$ *resonance at* $E_n = 3.76$ MeV. Experimentally [1,25]), a wide ($\Gamma \approx 300$ keV) resonance is seen at $E_n \approx 3.70$ MeV. However, both the cross-section fluctuation $\Delta\sigma$ and the *R*-matrix analysis of I suggest an assignment of 1^- for this state. The only nearby 3^- resonance seen experimentally [1]) is at $E_n \approx 4.126$ MeV. Unfortunately, the width of this resonance is only $\Gamma \approx 80$ keV, which is a factor of 3 smaller than the calculated width of $\Gamma \approx 210$ keV. Thus the identification of this state with the 3^- p-h resonance is somewhat doubtful. Another possibility would be a 3^- assignment for the state at $E_n \approx 4.25$, as suggested by Fossan *et al.* [19]). The *R*-matrix analysis of I is incompatible with a 3^- assignment, however. Finally, the state at $E_n \approx 4.64$ MeV with $J \geqq 2$ is also a candidate for identification with the 3^- p-h resonance. Although this state lies about 900 keV above the calculated 3^- resonance, its width ($\Gamma > 150$ keV) is more in accord with the theoretical value than that of the state at $E_n = 4.126$ MeV.

5.1.2. *The* $(2s_{\frac{1}{2}}\, p_{\frac{3}{2}}^{-1})_1$- *resonance* † *at* $E_n = 4.89$ MeV. This resonance is expected to exhibit an interference pattern characteristic of an s-wave. No resonances which show a clear interference with the background are observed above $E_n = 3.5$ MeV. However, it should be noted that such interference effects may be difficult to observe because of the problems of energy resolution and overlapping resonances. Because of the very crude contact force which we use, the predicted p-h resonance energies could be in error by 1–2 MeV. Alternatively, one can try to identify 1^- p-h states by comparing observed resonances in n+^{15}N with $T = 1$ levels seen in ^{16}O(γ, n)^{15}O. In the region of interest here, photoneutron peaks are seen at 19.08, 19.5 and 21 MeV c.m. energy in ^{16}O. The first peak lies in the neighborhood of a wide 1^- resonance in n+^{15}N at 18.28 MeV ($E_n = 3.70$ MeV), but the assignment of $J = 2^+$ seems well established for the 19.08 MeV state [9]). The peak at 19.5 MeV also does not seem to be identifiable as a p-h resonance [3]). Only the 21 MeV resonance in ^{16}O ($E_n = 6.6$ MeV in n+^{15}N) is a reasonable candidate for identification with the $(2s_{\frac{1}{2}}\, p_{\frac{3}{2}}^{-1})_1$- p-h state [refs. [3, 9])]. Thus on energetic grounds, as well as on the basis of the coupled channel calculation, it does not seem possible to identify the wide 1^- resonance at $E_n = 3.70$ MeV with the $(2s_{\frac{1}{2}}\, p_{\frac{3}{2}}^{-1})_1$- configuration. The small resonances at $E_n = 6.28$, 6.42 and 6.65 MeV, on the other hand, are all consistent with $J = 1$ and could be components of the p-h state. This hypothesis is supported by a consideration of the energy-averaged cross sections of fig. 6 of I. For averaging intervals of 300 or 500 keV, the above three components merge into a single peak at $E_n = 6.5$ MeV, very close to the energy $E_n = 6.6$ MeV expected for the $(2s_{\frac{1}{2}}\, p_{\frac{3}{2}}^{-1})_1$- state.

5.1.3. *The* $(d_{\frac{5}{2}}\, p_{\frac{3}{2}}^{-1})_2$- *resonance at* $E_n = 5.02$ MeV. The most promising candidate for identification with this resonance is the wide state seen experimentally at $E_n = 4.25$ MeV. The calculated width of $\Gamma \approx 120$ keV is somewhat smaller than the value $\Gamma = 300$ keV obtained in ref. [25]). However, the experimental level lies closer to the $(d_{\frac{5}{2}}\, p_{\frac{1}{2}}^{-1})_2$- p-h resonance than the calculated one, and the larger width could be due to a greater admixture of the $d_{\frac{5}{2}}$ single-particle resonance.

Another candidate is the wide ($\Gamma > 150$ keV) resonance at $E_n = 4.64$ MeV with $J = 2$. Further comment is futile without a firm spin and parity assignment for this state.

One could also suppose that the 2^- p-h resonance is fragmented, and search for a number of small components whose total width is roughly equal to the calculated width ††. Narrow resonances consistent with $J = 2$ are seen experimentally at $E_n = 4.8$, 5.06 and 5.9 MeV with widths of $\Gamma \approx 40$, 25 and 70 keV, respectively.

† As in ^{16}O calculations [3–8, 30–32]), the $(1d_{\frac{5}{2}}\, p_{\frac{3}{2}}^{-1})_1$- state lies above the $(2s_{\frac{1}{2}}\, p_{\frac{3}{2}}^{-1})_1$- state, although the unperturbed energies are reversed. This has been verified by following the trajectories of the resonance poles as a function of the coupling strength V_0.

†† The expected sum rule is that the total width of the calculated p-h resonance is about equal to the sum of the total widths of the fragments. Such a sum rule must be viewed with caution since (i) if the fragments are appreciably split in energy, one must consider the influence of penetration effects on the widths (ii) the 2p-2h states which mix with the p-h resonance also have a natural width which should be included in the sum rule.

These three resonances have a summed width of 135 keV and a center of gravity at $E_n = 5.25$ MeV. The good agreement with the calculated p-h resonance may be fortuitous.

5.1.4. *The* $(2s_{\frac{1}{2}}\, p_{\frac{3}{2}}^{-1})_{2^-}$ *resonance at* $E_n = 7.3$ MeV. The experimental cross section in the region around $E_n = 7.3$ MeV is quite complicated. However, if the cross section is averaged over a sufficiently large energy interval ($\Delta = 500$ keV in fig. 6 of I), a single broad resonance around $E_n = 7.3$ MeV emerges. It is very tempting to identify this energy-averaged structure with the calculated p-h resonance at the same energy but see subsect. 5.1.5 below. The calculated total cross section of about 1.2 b at $E_n = 7.3$ MeV agrees reasonably well with the experimental value of 1.45 b. The remaining discrepancy is certainly due in part to our omission of the inelastic channels ($\frac{1}{2}^+$ and $\frac{3}{2}^+$ in ^{15}N) which open up at $E_n = 5.65$ and 5.67.

5.1.5. *The* $(d_{\frac{5}{2}}\, p_{\frac{3}{2}}^{-1})_{1^-}$ *resonance at* $E_n = 7.75$ MeV. In ^{16}O, this component is observed at 22.3 MeV, corresponding to $E_n = 7.3$ MeV if we use the Coulomb energy of ref. [20]) and $E_n = 8$ MeV if the value given in sect. 4 is used. Thus the 1^- p-h resonance could conceivably be identified with either of the broad peaks seen in the energy averaged cross section at $E_n = 7.3$ or 8.5 MeV. Although the calculation suggests $J = 2^-$ for the peak at 7.3 MeV (see subsect. 5.1.4), the calculated energy is not reliable to better than ± 1–1.5 MeV. Thus we could have either $J = 1^-, 2^-$ or $2^-, 1^-$ for the peaks at $E_n = 7.3$ and 8.5 MeV.

5.1.6. *The* $(d_{\frac{5}{2}}\, p_{\frac{3}{2}}^{-1})_{0^-1^-2^-3^-}$ *resonances.* Because of the increased force strength V_0 which we have used, as compared to refs. [8,20–24]), these resonances are no longer visible in the theoretical cross section of fig. 2. Although the experimental cross section still displays considerable structure between $9 \leqq E_n \leqq 16$ MeV, the energy averaged cross section (fig. 6 of I with $\Delta = 500$, 1000 keV) exhibits only one clearly defined resonance at about $E_n = 9.7$ MeV. This resonance arises from two prominent peaks at $E_n = 9.61$ and 9.77 MeV (see table 1 of I) with spins $J \geqq 3$, and hence one is tempted to identify this structure with the $(d_{\frac{5}{2}}\, p_{\frac{3}{2}}^{-1})_{3^-}$ p-h configuration. Indeed, some previous calculations [12,20–21]) have placed this 3^- state in the region $9.5 \leqq E_n \leqq 10$ MeV.

In the reaction ^{16}O$(\gamma, n)^{15}$O, the prominent peak at $E = 24.3$ MeV is usually interpreted as the $(d_{\frac{5}{2}}\, p_{\frac{3}{2}}^{-1})_{1^-}$ p-h state [9]). In n+^{15}N, the 1^- state should thus appear at about 10.1 MeV. Unfortunately, the presence of the two large peaks ($J \geqq 3$) discussed above would tend to mask the effects of a further broad 1^- peak in this region.

Finally, there seems to be no evidence that the $(d_{\frac{5}{2}}\, p_{\frac{3}{2}}^{-1})_{0^-2^-}$ configurations are seen experimentally. Several very broad undulations still visible in the average cross section above $E_n = 11$ MeV cannot be meaningfully associated with these resonances.

5.2. EFFECT OF VARYING THE SINGLE-PARTICLE POTENTIAL

To explore the sensitivity of the results to the choice of single-particle potential, calculations have also been performed with potentials other than those listed in table 1. For example, a Woods-Saxon plus Coulomb potential was used to generate the $p_{\frac{1}{2}}^{-1}$

and $p_{\frac{1}{2}}^{-1}$ proton-hole wave functions, the depths of the Woods-Saxon potential being readjusted so as to reproduce the correct binding energies. The total cross section obtained is practically identical to that of fig. 2, indicating that Coulomb effects are unimportant. In addition, the depth of the p-wave potential for the continuum has been varied between 48 and 60 MeV, other parameters of pot. A being kept fixed.

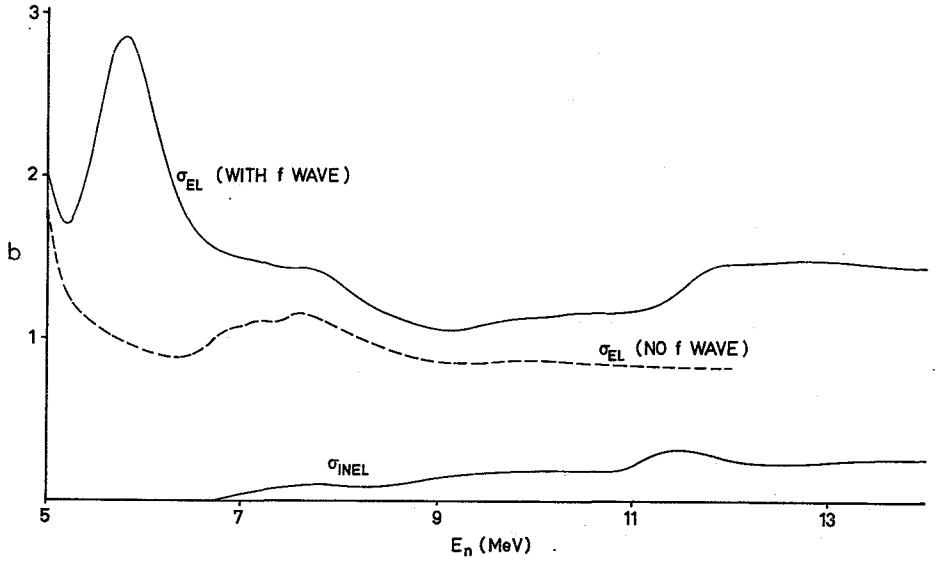

Fig. 4. Calculated elastic (upper solid curve) and inelastic (lower solid curve) total cross sections using $V_0 = 925$ MeV · fm^3, $g = 0.312$ and the parameters of potential C. The total cross section obtained using potential A (dashed line) is given for comparison. The difference in cross section is due to the inclusion of $l = 3$ in potential C.

The magnitude of the total cross section varies somewhat, but the positions and widths of the p-h resonances remain unaffected.

5.3. EFFECT OF HIGHER PARTIAL WAVES

The calculations described in subsects. 5.1 and 5.2 have included only s-, p-, and d-waves in the continuum. In this section, we investigate effects due to higher partial waves.

It has been suggested in ref. [19]) that the prominent resonance at $E_n \approx 5.73$ MeV may be due to the $(1f_{\frac{7}{2}}\, 1p_{\frac{1}{2}}^{-1})$ configuration. To investigate this possibility, we have performed calculations including the f-wave. We first adjusted the $l = 3$ well depth so that a single-particle resonance was obtained at the energy of the $f_{\frac{7}{2}}$ single-particle state given in refs. [17,18]). The 3^+ and 4^+ resonances arising from the $(f_{\frac{7}{2}}\, p_{\frac{1}{2}}^{-1})$ coupling then lie at $E_n = 4.02$ and 3.8 MeV, respectively, with widths of $\Gamma \approx 250$ keV. No resonances which are likely to have $J = 4$ are seen experimentally in this region. This suggests that the $1f_{\frac{7}{2}}$ single-particle energy given in refs. [17,18]) is inappropriate

here. We then adjusted the $l = 3$ well depth so that the solution of the coupled equations yielded the 4^+ resonance at the desired energy of $E_n = 5.73$ MeV. The total elastic cross section obtained with this potential (C) is shown in fig. 4. The 3^+ and 4^+ resonances are practically degenerate ($E_n = 5.9$ and 5.73 MeV, respectively), so that they merge into one bump in the total cross section with a peak at $E_n \approx 5.77$ MeV. The peak cross section of 2.86 b agrees well with that of the large resonance seen experimentally at $E_n = 5.73$ MeV. However, the 3^+ and 4^+ resonances both have calculated widths of $\Gamma \approx 750$ keV, while the resonance seen experimentally [19]) has $\Gamma \approx 165$ keV. This indicates that at best only some fraction of the $(f_{\frac{7}{2}}\, p_{\frac{1}{2}}^{-1})$ configuration is present in the resonance at $E_n \approx 5.73$ MeV. The uncertainty in the value for the $f_{\frac{7}{2}}$ single-particle energy renders even this modest conclusion somewhat dubious.

In ref. [19]), it is also suggested that the narrow ($\Gamma \leqq 30$ keV) resonance seen at $E_n \approx 5.42$ MeV is perhaps due to the $(1d_{\frac{5}{2}}\, 1p_{\frac{3}{2}}^{-1})_{4^-}$ configuration. In order for this state to have a width in our model, we must include continua with $l \geqq 4$. We have performed calculations with potential D which includes the g-wave. The 4^- resonance was found at an energy $E_n = 6.325$ MeV with a width of $\Gamma \approx 1.1$ keV. There would be no chance of observing such a resonance, since the experimental energy resolution is about 20 keV in this region.

5.4. ANGULAR DISTRIBUTIONS

In fig. 5, the calculated angular distributions are compared with experiment in the region $2 \leqq E_n \leqq 3$ MeV of the $d_{\frac{3}{2}}$ single-particle resonance. The agreement with experiment is reasonably good except that the calculated cross sections have a tendency to be somewhat low for backward angles.

The calculated coefficients B_L of the expansion

$$\frac{d\sigma}{d\Omega} = \sum_L B_L P_L(\cos\Theta)$$

are shown in fig. 6, together with experimental results taken from refs. [1,26]).

6. Summary

We have presented the results of a calculation of the total and differential cross sections for the reaction $^{15}N(n, n)^{15}N$ using the method of coupled channels. A simple contact force for the residual interaction was used, and calculations were restricted to a 1p-1h configuration space.

The main success of the model is in the region of the $d_{\frac{3}{2}}$ single-particle resonance. The strength and spin mixture of the residual interaction were adjusted so that the 1^- and 2^- resonances arising from the $(d_{\frac{3}{2}}\, p_{\frac{1}{2}}^{-1})$ configuration are found at $E_n = 2.3$ and 2.9 MeV, respectively, corresponding to experimentally observed wide resonances of the same spin and parity [1,25]). With this choice of residual force, the absolute magnitude of the cross section and the angular distributions are in good agreement with experiment in the region $2 \leqq E_n \leqq 3$ MeV.

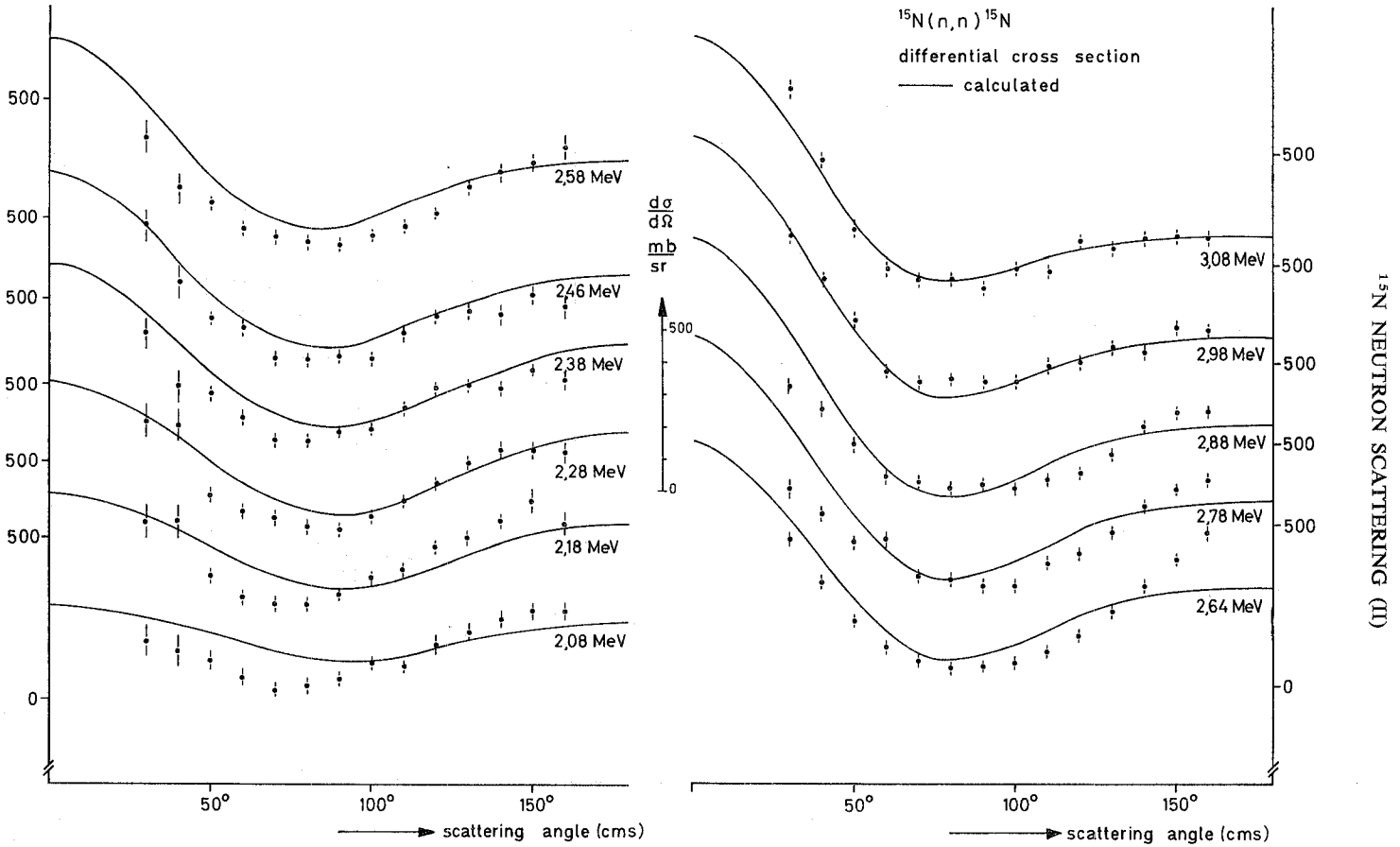

Fig. 5. Angular distributions in the region of the $d_{\frac{3}{2}}$ single-particle resonance. The solid curves were calculated with $V_0 = 970$ MeV · fm^3, $g = 0.312$ using potential A. The experimental points (shown as dots) are taken from I. Each curve is labelled with the corresponding lab. energy.

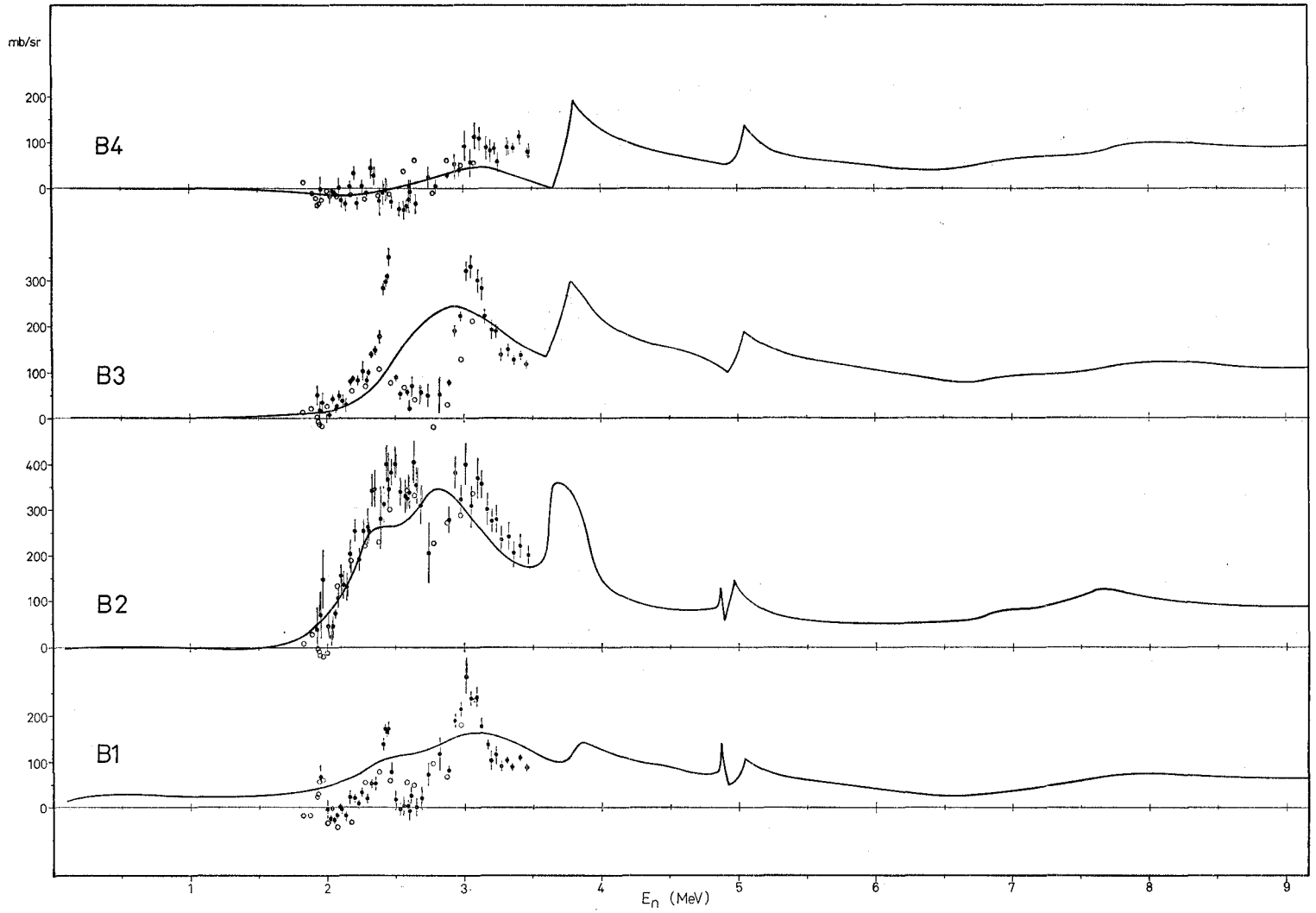

Fig. 6. Coefficients B_L in an expansion of the differential cross section in Legendre polynomials. The solid lines are the results of calculations

The main weakness of the model is the omission of 2p-2h (and more complicated) configurations. Although the number of resonances seen in the compound system ^{16}N is not particularly large, there are still many more states observed than are predicted by the p-h model. However, the p-h model is capable of describing the *energy-averaged* cross section. The averaging interval Δ must be sufficiently large so that the narrow compound resonances are smoothed out. Indeed, when $\Delta \geqq 300$ keV, four broad peaks emerge in the energy region $6 \leqq E_n \leqq 10$ MeV, which have been tentatively identified with the $(2s_{\frac{1}{2}}\, p_{\frac{3}{2}}^{-1})_{1^-,2^-}$, $(d_{\frac{5}{2}}\, p_{\frac{3}{2}}^{-1})_{1^-}$ and $(d_{\frac{3}{2}}\, p_{\frac{3}{2}}^{-1})_{3^-}$ p-h configurations. The p-h calculation also reproduces the magnitude of the average cross section in this region, when allowance is made for the effect of inelastic channels.

It should be noted that not all resonances which have an appreciable width Γ are explainable in terms of the p-h model. Two examples are the 1^+ and 1^- resonances at $E_n = 2.93$ and 3.70 MeV with $\Gamma = 260$ and 300 keV, respectively. Even if these states are predominantly of 2p-2h character, their large width could be due to an appreciable admixture of the nearby $d_{\frac{3}{2}}$ single-particle resonance.

Thanks are due to R. H. Lemmer, C. Mahaux and H. A. Weidenmüller for many discussions. Most of the numerical calculations were performed on the CDC 3300 at the Max-Planck Institut für Kernphysik in Heidelberg.

References

1) B. Zeitnitz *et al.*, Nucl. Phys. **A166** (1971) 443
2) T. Tamura, Ann. Rev. of Nucl. Sci., ed. E. Segrè, J. Grover and H. P. Noyes (Ann. Reviews, Palo Alto, California) Vol. **19** (1969) p. 99, and other references cited therein
3) B. Buck and A. D. Hill, Nucl. Phys. **A95** (1967) 271
4) J. Raynal, M. A. Melkanoff and T. Sawada, Nucl. Phys. **A101** (1967) 369
5) A. M. Saruis and M. Marangoni, Nucl. Phys. **A132** (1969) 433
6) V. Gillet and N. Vinh-Mau, Nucl. Phys. **54** (1964) 321
7) J. P. Elliott and B. H. Flowers, Proc. Roy. Soc. **A242** (1957) 57
8) G. E. Brown, L. Castillejo and J. A. Evans, Nucl. Phys. **22** (1961) 1
9) B. M. Spicer, in Advances in nuclear physics, vol. **2**, ed. M. Baranger and E. Vogt (Plenum Press, New York, 1969) p. 1, and references cited therein
10) V. Gillet, M. A. Melkanoff and J. Raynal, Nucl. Phys. **A97** (1967) 631
11) C. A. Caine and R. H. Lemmer, Tech. Report No. 78, AT (30-1)-2098-113, MIT, November 1964, unpublished
12) C. B. Dover and P. Sandner, Phys. Lett. **29B** (1969) 405
13) E. H. Auerbach, C. B. Dover, A. K. Kerman, R. H. Lemmer and E. H. Schwarcz, Phys. Rev. Lett. **17** (1966) 1184
14) D. Agassi, V. Gillet and A. Lumbroso, Nucl. Phys. **A130** (1969) 129
15) J. S. Lopes, O. Häusser, H. J. Rose, A. R. Poletti and M. F. Thomas, Nucl. Phys. **76** (1966) 223
16) F. Ajzenberg-Selove and T. Lauritsen, Nucl. Phys. **11** (1959) 1
17) J. M. Eisenberg, B. M. Spicer and M. E. Roe, Nucl. Phys. **71** (1965) 273
18) B. M. Spicer and J. M. Eisenberg, Nucl. Phys. **63** (1965) 520
19) D. B. Fossan, R. A. Chalmers, S. R. Salisbury and F. J. Vaughn, Phys. Rev. **152** (1966) 980
20) R. H. Lemmer and C. Shakin, Ann. of Phys. **27** (1964) 13
21) W. Ebenhöh, W. Glöckle, J. Hüfner and H. A. Weidenmüller, Z. Phys. **202** (1967) 301
22) W. Ebenhöh and B. L. Andersen, Nucl. Phys. **A127** (1969) 209

23) B. Pöpel and G. Schütte, Z. Phys. **231** (1970) 48
24) J. Hüfner and R. H. Lemmer, Phys. Rev. **175** (1968) 1394
25) P. V. Hewka, C. H. Holbrow and R. Middleton, Nucl. Phys. **88** (1966) 561
26) C. P. Sikkema, Nucl. Phys. **32** (1962) 470
27) D. B. Fossan, R. A. Chalmers, L. F. Chase and S. R. Salisbury, Phys. Rev. **135** (1964) B1347
28) T. R. Donoghue, A. F. Behof and S. E. Darden, Nucl. Phys. **54** (1964) 49
29) H. Feshbach, A. K. Kerman and R. H. Lemmer, Ann. of Phys. **41** (1967) 230
30) H. A. Mavromatis, W. Markiewicz and A. M. Green, Nucl. Phys. **A90** (1967) 101
31) J. D. Perez and W. M. MacDonald, Phys. Rev. **182** (1969) 1066
32) S. M. Perez, Nucl. Phys. **A136** (1969) 599